HOKKAIDO UNIVERSITY

Title	Low-energy structure and β-decay properties of neutron-rich nuclei in the region of a shape phase transition
Author(s)	Nomura, Kosuke
Citation	Physical Review C, 109(3), 034319 https://doi.org/10.1103/PhysRevC.109.034319
Issue Date	2024-03-27
Doc URL	https://hdl.handle.net/2115/92570
Rights	©2024 American Physical Society
Type	journal article
File Information	PhysRevC.109.034319.pdf

Hokkaido University Collection of Scholarly and Academic Papers : HUSCAP

Low-energy structure and β-decay properties of neutron-rich nuclei in the region of a shape phase transition

Kosuke Nomura*
Department of Physics, Hokkaido University, Sapporo 060-0810, Japan
and Nuclear Reaction Data Center, Hokkaido University, Sapporo 060-0810, Japan

(Received 28 December 2023; accepted 6 March 2024; published 27 March 2024)

The low-energy structure and β-decay properties of the neutron-rich even-mass nuclei near the neutron number $N = 60$ that are experimentally of much interest are investigated within the framework of the nuclear density functional theory and the interacting boson-fermion-fermion model. By using the results of the constrained self-consistent mean-field calculations based on the relativistic energy density functional, the interacting-boson Hamiltonian describing the even-even core nuclei, the boson-fermion, and the fermion-fermion interactions are determined. The Gamow-Teller transition strengths, with the corresponding operator being constructed without introducing further phenomenological adjustment, are computed by using the wave functions of the initial and final nuclei of the β decay. The triaxial quadrupole potential energy surfaces computed for the $N = 60$ even-even isotones suggest a pronounced γ softness. The calculated energy spectra for the even-even and odd-odd nuclei in the Rb to Cd isotopic chains exhibit an abrupt change in nuclear structure around $N = 60$, as suggested experimentally. The predicted β-decay $\log_{10} ft$ values underestimate the measured values for the nuclei with low Z and with $N \leqslant 60$, exhibit a rapid increase for $N > 60$, reflecting the nuclear structure evolution, and agree rather well with the measured values for those nuclei with Z being not far from the proton major shell closure $Z = 50$. Sensitivity of the predicted β-decay properties to the model assumptions and parameters employed in the nuclear structure calculations is discussed, specifically, by comparing results obtained based on the different choices of the underlying energy density functional.

DOI: 10.1103/PhysRevC.109.034319

I. INTRODUCTION

The low-energy structure of neutron-rich heavy nuclei with the neutron number $N \approx 60$ and with the mass $A \approx 100$ has been of much interest from both experimental and theoretical points of view. In these nuclear systems a subtle interplay between the single-particle and collective degrees of freedom plays an essential role. The nuclear structure phenomena that are extensively studied in this mass region include the abrupt change of nuclear shapes around $N = 60$, often referred to as quantum phase transitions [1], the coexistence of different intrinsic shapes [2] in the neighborhood of the ground state and corresponding low-lying excited 0^+ states. Experiments using radioactive-ion beams have been carried out to reveal properties of those neutron-rich nuclei that are even heavier and beyond the region of shape phase transitions at $N \approx 60$. Theoretical predictions for the neutron-rich nuclei in this region have been made extensively with a number of nuclear structure models, such as the nuclear shell model [3–6], methods based on the nuclear energy density functional (EDF) [7–11], and the interacting boson model (IBM) [12–16].

Along with their nuclear structure aspects, the neutron-rich heavy nuclei are also relevant to astrophysical nucleosynthesis processes, i.e., the rapid neutron-capture (r) process and β decay. The β-decay rate should be sensitive to the wave functions for the initial and final nuclei of the process, which vary significantly from one nucleus to another in the transitional regions. Reliable theoretical descriptions, as well as precise measurements [17–21], are key to evaluate the nuclear β-decay matrix elements and hence to model the astrophysical process producing heavy chemical elements. Consistent descriptions of the nuclear low-lying structure and β decay have been provided by several theoretical approaches such as the interacting boson-fermion and boson-fermion-fermion models (IBFM and IBFFM) [22–29], the quasiparticle random-phase approximations [30–38], and the nuclear shell model [3,39–41].

Furthermore, what is worth mentioning is the double-β decay, a rare process in which single-β decay occurs successively between the neighboring even-even nuclei, emitting two electrons (or positrons) and some light particles such as neutrinos [42–44]. In particular, should that type of the double-β decay that does not emit neutrinos (i.e., neutrinoless double-β decay; $0\nu\beta\beta$) be observed by experiment, it would provide crucial pieces of information about the masses and the nature of neutrinos, and the validity of various symmetry requirements for the electroweak fundamental interaction. Since the predicted $0\nu\beta\beta$ nuclear matrix elements (NMEs) differ by several factors among different theoretical approaches, tremendous efforts have been devoted to reduce and control the theoretical uncertainties inherent to the models employed.

*nomura@sci.hokudai.ac.jp

 ©2024 American Physical Society

The study of the single-β decay is also instrumental for predicting accurately the double-β NMEs, especially when it is necessary to compute intermediate states of the odd-odd nuclei without assuming the closure approximation.

Among the theoretical models describing β decay, as well as nuclear structure, the IBM, a model in which correlated monopole and quadrupole pairs of valence nucleons are represented by s and d bosons, respectively [12,45,46], has been quite successful in the quantitative description of the quadrupole collective states of medium-heavy and heavy even-even nuclei. In the conventional IBM studies, calculations have been purely phenomenological, since the parameters of the Hamiltonian have been obtained from experiment. On the other hand, the IBM should be rooted in the underlying microscopic nuclear structure, and the model Hamiltonian has been shown to be derived from nucleonic degrees of freedom [12,45–48]. In particular, a fermion-to-boson mapping technique has been developed [48], in which the IBM Hamiltonian is completely determined by using the results of the self-consistent mean-field (SCMF) calculation that is based on a given EDF. This method has been applied to a number of studies on the quadrupole collective states [48–51]. An extension of the method to those nuclear systems with odd numbers of neutrons and/or protons has been made by incorporating the particle-boson coupling, with microscopic input provided by the same EDF calculations [52,53]. In these cases, in addition to the IBM Hamiltonian describing an even-even nucleus, unpaired nucleon degrees of freedom and their coupling to the even-even boson core should be considered in the framework of the IBFM or IBFFM. The IBFM and IBFFM formulated in that way have also been employed to study β decay of the γ-soft nuclei near the Ba and Xe regions [27,28], the neutron-deficient Ge and As nuclei [54], the neutron-rich Pd and Rh nuclei [55], and the two-neutrino double-β ($2\nu\beta\beta$) decay in a large number of the candidate nuclei [56].

This article presents a simultaneous description of the low-energy collective excitations and β-decay properties of the neutron-rich nuclei in the vicinity of $N = 60$, which is experimentally of much interest, within the mapped IBM framework mentioned above. The scope of the analysis is to study the correlations between the changes in the nuclear structure of the initial and final even-even nuclei and the predictions of the β decay. The present study covers the even-even and odd-odd nuclei from the proton number $Z = 36$ (Kr) to 48 (Cd) isotopes with the neutron number $54 \leqslant N \leqslant 64$, in which region rapid shape phase transitions are expected to occur. It is noted that the present analysis is restricted to the allowed β decay, i.e., the transition in which parity is conserved and that takes place between those states with angular momenta I differing by $\Delta I \leqslant 1$. Note also that only the β decay between positive-parity states is considered. In addition, some of the nuclei included in the present analysis are also candidates for the $0\nu\beta\beta$ decay, e.g., ^{96}Zr and ^{100}Mo. Their structure and single-β and double-β properties have already been studied in a previous paper [56], and some updated results on these particular nuclei are included in the present article.

The paper is organized as follows. In Sec. II, the theoretical framework to describe low-lying states of the considered even-even and odd-odd nuclei is presented, followed by the definition of the β-decay operator. In Sec. III, results of the SCMF calculations along the $N = 60$ isotones, and of the spectroscopic calculations on the low-spin and low-energy spectra, and some electromagnetic transition properties of the considered nuclei are discussed. In Sec. IV, results of the β-decay properties, and the sensitivity of the final results to the choice of the EDF, are discussed. A summary of the main results and conclusions are given in Sec. V.

II. THEORETICAL FRAMEWORK

A. Self-consistent mean-field method

As the first step, the constrained SCMF calculations are performed for a set of even-even Kr, Sr, Zr, Mo, Ru, Pd, and Cd isotopes with $54 \leqslant N \leqslant 64$ by means of the relativistic Hartree-Bogoliubov (RHB) method [8,9,57,58]. For the particle-hole channel, the density-dependent point coupling (DD-PC1) EDF [59] is employed, which is widely used in microscopic calculations on nuclear structure and dynamics [9]. For the particle-particle channel the separable pairing force of finite range [60] is considered with the strength 728 MeV fm^3, which has been determined to reproduce the pairing gap obtained from the Gogny D1S [61] interaction. The sensitivity of the mean-field results on various intrinsic properties to the choice of relativistic EDF and to the strength of this pairing force has been extensively studied, e.g., in Ref. [62].

Here the particular choice of the relativistic EDF and the pairing interaction is made as the microscopic input to the mapped IBM-2, since these combinations have been shown to be adequate in a number of nuclear structure studies in different mass regions concerning, e.g., the octupole deformations and collectivity [63–65], and the structural evolution in neutron-rich even-even and odd-mass Zr isotopes [15], and in the systematic calculation of the double-β decay of 26 even-even nuclei [56] and single-β decay in transitional As and Ge nuclei [54]. As in the case of these previous RHB plus IBM-2 studies, the constraints imposed in the present RHB SCMF calculations are on the expectation values of the mass quadrupole moments $\hat{Q}_{20}$ and $\hat{Q}_{22}$, which are related to the polar deformation variables β and γ representing degrees of axial deformation and triaxiality, respectively [66]. The SCMF calculations provide intrinsic properties such as the potential energy surfaces (PESs) defined in terms of the triaxial quadrupole deformations (β, γ), and single-particle energies and occupation probabilities. These quantities are used as a microscopic input for the spectroscopic calculations, as described below.

B. Interacting boson-fermion-fermion model

Within the mean-field approximations some important symmetries, such as the rotational invariance and conservation of particle numbers, are broken. To study physical observables in the laboratory frame such as the excitation energies and electromagnetic transition rates, it is necessary to go beyond the SCMF level [67], by taking into account the dynamical correlations arising from the restorations of symmetries and from the inclusion of quantum fluctuations around the mean-field solution, which are not taken into account properly

in the mean-field approximation. Such a beyond-mean-field treatment is here made by means of the IBM.

In the present analysis the neutron-proton version of the IBM (IBM-2) is considered, which consists of the neutron and proton bosons reflecting the collective neutron and proton pairs from a microscopic point of view [12,45,46]. The numbers of neutron, N_ν, and proton, N_π, bosons are conserved separately, and are equal to half the numbers of valence neutron and proton pairs, respectively. Here the ^{78}Ni doubly magic nucleus is taken as the inert core for describing the even-even Kr, Sr, Zr, Mo, Ru, Pd, and Cd nuclei. The distinction between the neutron and proton bosons is made also in the IBFFM, denoted hereafter as IBFFM-2. The IBFFM-2 Hamiltonian is given in general as

$$\hat{H} = \hat{H}_{\rm B} + \hat{H}_{\rm F}^{\nu} + \hat{H}_{\rm F}^{\pi} + \hat{V}_{\rm BF}^{\nu} + \hat{V}_{\rm BF}^{\pi} + \hat{V}_{\nu\pi}. \tag{1}$$

The first term on the right-hand side of the above equation denotes the IBM-2 Hamiltonian describing the even-even nucleus, and is of the form

$$\begin{aligned}\hat{H}_{\rm B} = {} & \epsilon_d\big(\hat{n}_{d_\nu} + \hat{n}_{d_\pi}\big) + \kappa \hat{Q}_\nu \cdot \hat{Q}_\pi \\ & + \kappa_\nu \hat{Q}_\nu \cdot \hat{Q}_\nu + \kappa_\pi \hat{Q}_\pi \cdot \hat{Q}_\pi + \kappa' \hat{L} \cdot \hat{L},\end{aligned} \tag{2}$$

where the first term stands for the d-boson number operator with $\hat{n}_{d_\rho} = d_\rho^\dagger \cdot \tilde{d}_\rho$ ($\rho = \nu$ or π) and with ϵ_d the single d boson energy. The second, third, and fourth terms are the quadrupole-quadrupole interactions between neutron and proton bosons, between neutron and neutron bosons, and between proton and proton bosons, respectively. The quadrupole operator $\hat{Q}_\rho$ is defined as $\hat{Q}_\rho = s_\rho^\dagger \tilde{d}_\rho + d^\dagger s_\rho + \chi_\rho (d_\rho^\dagger \times \tilde{d}_\rho)^{(2)}$, with χ_ν and χ_π being dimensionless parameters. κ, κ_ν, and κ_π are strength parameters.

Among the quadrupole-quadrupole interactions, the unlike-boson interaction, $\hat{Q}_\nu \cdot \hat{Q}_\pi$, makes a dominant contribution to low-lying collective states. For most of the nuclei considered in this study, the like-boson quadrupole-quadrupole interaction terms, $\hat{Q}_\nu \cdot \hat{Q}_\nu$ and $\hat{Q}_\pi \cdot \hat{Q}_\pi$, turn out to play a minor role, and are thus neglected by setting $\kappa_\nu = \kappa_\pi = 0$. These terms are, however, included for all the Zr isotopes considered and ^{100}Sr and ^{102}Sr isotopes. This choice is based on the peculiar nuclear structure and its evolution as a function of N in the neutron-rich Zr isotopes, as investigated in the earlier mapped IBM-2 with RHB calculations reported in Ref. [15]. In that study, these like-boson quadrupole-quadrupole interaction terms, as well as the unlike-boson one, have been introduced to better describe the low-energy structure at the quantitative detail. Since the RHB PESs for the ^{100}Sr and ^{102}Sr nuclei are more or less similar in topology to those for the neighboring Zr isotopes, the same interaction terms are introduced. In the following, for the above-mentioned nuclei a simple relation, $\kappa_\nu = \kappa_\pi = \kappa/2$, is assumed in order to reduce the number of parameters.

The fifth term on the right-hand side of Eq. (2) stands for a rotational term, with κ' being the strength parameter, and $\hat{L} = \hat{L}_\nu + \hat{L}_\pi$ denotes the angular momentum operator with $\hat{L}_\rho = (d_\rho^\dagger \times \tilde{d}_\rho^\dagger)^{(1)}$.

The second and third terms of Eq. (1) represent the single-neutron and -proton Hamiltonians, respectively, and take the form

$$\hat{H}_{\rm F}^{\rho} = -\sum_{j_\rho} \epsilon_{j_\rho} \sqrt{2j_\rho + 1} \big(a_{j_\rho}^\dagger \times \tilde{a}_{j_\rho}\big)^{(0)} \equiv \sum_{j_\rho} \epsilon_{j_\rho} \hat{n}_{j_\rho}, \tag{3}$$

where ϵ_{j_ρ} stands for the single-particle energy of the odd neutron ($\rho = \nu$) or proton ($\rho = \pi$) orbital j_ρ. $a_{j_\rho}^{(\dagger)}$ represents the particle annihilation (creation) operator, with $\tilde{a}_{j_\rho}$ defined by $\tilde{a}_{j_\rho m_\rho} = (-1)^{j_\rho - m_\rho} a_{j_\rho - m_\rho}$. On the right-hand side of Eq. (3), $\hat{n}_{j_\rho}$ stands for the number operator for the odd particle. The single-particle space taken in the present study comprises the neutron $3s_{1/2}$, $2d_{3/2}$, $2d_{5/2}$, and $1g_{7/2}$ orbitals, and the proton $1g_{9/2}$ orbital in the $N = 50 - 82$ and $Z = 28 - 50$ major oscillator shells for calculating the positive-parity states of the odd-odd nuclei.

The fourth (fifth) term on the right-hand side of Eq. (1) denotes the interaction between a single neutron (or proton) and the even-even boson core. A simplified form which was derived microscopically within the generalized seniority scheme [68,69] is here adopted:

$$\hat{V}_{\rm BF}^{\rho} = \Gamma_\rho \hat{V}_{\rm dyn}^{\rho} + \Lambda_\rho \hat{V}_{\rm exc}^{\rho} + A_\rho \hat{V}_{\rm mon}^{\rho}, \tag{4}$$

where the first, second, and third terms represent the quadrupole dynamical, exchange, and monopole interactions, respectively, with the strength parameters Γ_ρ, Λ_ρ, and A_ρ. Each term in the above expression reads

$$\hat{V}_{\rm dyn}^{\rho} = \sum_{j_\rho j_\rho'} \gamma_{j_\rho j_\rho'} \big(a_{j_\rho}^\dagger \times \tilde{a}_{j_\rho'}\big)^{(2)} \cdot \hat{Q}_{\rho'}, \tag{5}$$

$$\begin{aligned}\hat{V}_{\rm exc}^{\rho} = {} & -(s_{\rho'}^\dagger \times \tilde{d}_{\rho'})^{(2)} \cdot \sum_{j_\rho j_\rho' j_\rho''} \sqrt{\frac{10}{N_\rho (2j_\rho + 1)}} \beta_{j_\rho j_\rho'} \beta_{j_\rho'' j_\rho} : \\ & \times \Big[\big(d_\rho^\dagger \times \tilde{a}_{j_\rho''}\big)^{(j_\rho)} \times \big(a_{j_\rho'}^\dagger \times \tilde{s}_\rho\big)^{(j_\rho')}\Big]^{(2)} : + ({\rm H.c.}),\end{aligned} \tag{6}$$

$$\hat{V}_{\rm mon}^{\rho} = \hat{n}_{d_\rho} \hat{n}_{j_\rho}, \tag{7}$$

where the j-dependent factors $\gamma_{j_\rho j_\rho'} = (u_{j_\rho} u_{j_\rho'} - v_{j_\rho} v_{j_\rho'}) Q_{j_\rho j_\rho'}$, and $\beta_{j_\rho j_\rho'} = (u_{j_\rho} v_{j_\rho'} + v_{j_\rho} u_{j_\rho'}) Q_{j_\rho j_\rho'}$, with $Q_{j_\rho j_\rho'} = \langle \ell_\rho \tfrac{1}{2} j_\rho \| Y^{(2)} \| \ell_\rho' \tfrac{1}{2} j_\rho' \rangle$ being the matrix element of the fermion quadrupole operator in the single-particle basis. $\hat{Q}_{\rho'}$ in Eq. (5) denotes the quadrupole operator in the boson system, and was already introduced in Eq. (2). The notation $: (\cdots) :$ in Eq. (6) stands for normal ordering. Note that the forms of $\hat{V}_{\rm BF}^{\nu}$ and $\hat{V}_{\rm BF}^{\pi}$ are considered based on the assumption [68,69] that among the boson-fermion interactions those between unlike particles [i.e., between a neutron (proton) and proton (neutron) bosons] are most important for the quadrupole dynamical and exchange terms, and those between like particles [i.e., between a neutron (proton) and neutron (proton) bosons] are relevant for the monopole term. It is also noted that within the seniority considerations the unperturbed single-particle energy for the orbital j_ρ, ϵ_{j_ρ}, in Eq. (3) should be replaced with the quasiparticle energy, denoted $\tilde{\epsilon}_{j_\rho}$.

The last term of the IBFFM-2 Hamiltonian (1), $\hat{V}_{\nu\pi}$, corresponds to the residual interaction between the unpaired neutron and proton. The following form is considered for this

interaction:

$$\hat{V}_{\nu\pi} = 4\pi(v_{\rm d} + v_{\rm ssd}\boldsymbol{\sigma}_\nu \cdot \boldsymbol{\sigma}_\pi)\delta(\boldsymbol{r})\delta(\boldsymbol{r}_\nu - r_0)\delta(\boldsymbol{r}_\pi - r_0) - \frac{1}{\sqrt{3}}v_{\rm ss}\boldsymbol{\sigma}_\nu \cdot \boldsymbol{\sigma}_\pi + v_{\rm t}\left[\frac{3(\boldsymbol{\sigma}_\nu \cdot \mathbf{r})(\boldsymbol{\sigma}_\pi \cdot \mathbf{r})}{r^2} - \boldsymbol{\sigma}_\nu \cdot \boldsymbol{\sigma}_\pi\right]. \tag{8}$$

The first term consists of the δ, and spin-spin δ terms, while the second and third terms represent, respectively, the spin-spin and tensor interactions. $v_{\rm d}$, $v_{\rm ssd}$, $v_{\rm ss}$, and $v_{\rm t}$ are strength parameters. Note that $\boldsymbol{r} = \boldsymbol{r}_\nu - \boldsymbol{r}_\pi$ is the relative coordinate of the neutron and proton, and $r_0 = 1.2A^{1/3}$ fm. The matrix element of $\hat{V}_{\nu\pi}$, denoted by $V'_{\nu\pi}$, has the following (u, v)-dependent form [25]:

$$\hat{V}'_{\nu\pi} = \left(u_{j'_\nu}u_{j'_\pi}u_{j_\nu}u_{j_\nu} + v_{j'_\nu}v_{j'_\pi}v_{j_\nu}v_{j_\nu}\right)V^J_{j'_\nu j'_\pi j_\nu j_\pi} - \left(u_{j'_\nu}v_{j'_\pi}u_{j_\nu}v_{j_\pi} + v_{j'_\nu}u_{j'_\pi}v_{j_\nu}u_{j_\pi}\right) \times \sum_{J'}(2J'+1)\begin{Bmatrix} j'_\nu & j_\pi & J' \\ j_\nu & j'_\pi & J \end{Bmatrix} V^{J'}_{j'_\nu j_\pi j_\nu j'_\pi}, \tag{9}$$

with

$$V^J_{j'_\nu j'_\pi j_\nu j_\pi} = \langle j'_\nu j'_\pi; J|\hat{V}_{\nu\pi}|j_\nu j_\pi; J\rangle \tag{10}$$

being the matrix element between the bases defined in terms of the neutron-proton pair coupled to the angular momentum J. The bracket in Eq. (9) represents the Racah coefficient. By following the procedure of Ref. [70], those terms resulting from contractions are neglected in Eq. (9).

C. Procedure to build the IBFFM-2 Hamiltonian

The procedure to determine the IBFFM-2 Hamiltonian (1) consists in the following three steps.

(i) First, the IBM-2 Hamiltonian is determined in such a way that the (β, γ) PES obtained from the constrained SCMF calculation is mapped onto the corresponding one in the IBM system which is represented as the energy expectation value in the boson coherent state [71]. This procedure specifies optimal parameters of the IBM-2 that renders the IBM-2 PES as similar as possible to the SCMF one. Only the strength parameter κ' for the $\hat{L}\cdot\hat{L}$ term [see Eq. (2)] is determined separately so that the cranking moment of inertia calculated in the boson intrinsic state at the equilibrium minimum is equal to the Inglis-Belyaev (IB) moment of inertia obtained with the RHB calculation. The IB moment of inertia is here increased by 30%, taking into account the fact that it considerably underestimates the observed moments of inertia. See Refs. [48–50] for details about the determination of the IBM-2 Hamiltonian.

(ii) The single-fermion Hamiltonian, $\hat{H}_{\rm F}$ [Eq. (3)], and boson-fermion interactions, $\hat{V}_{\rm BF}$ [Eq. (4)], are constructed by using the procedure of Ref. [52]: The SCMF RHB calculations are performed for the neighboring odd-N or odd-Z nucleus with the constraint on zero deformation to provide quasiparticle energies, $\tilde{\epsilon}_{j_\rho}$, and occupation probabilities, $v^2_{j_\rho}$, at the spherical configuration for the odd nucleon at orbitals j_ρ. These quantities are then input to $\hat{H}^\rho_{\rm F}$ and $\hat{V}^\rho_{\rm BF}$, respectively. The remaining three coupling constants, Γ_ρ, Λ_ρ, and A_ρ, are determined to fit the experimental data for a few low-lying positive-parity levels of each odd-N and odd-Z nuclei. Table I summarizes the even-even, neighboring odd-N, odd-Z, and odd-odd nuclei studied in this paper. It is worth mentioning that Y nuclei, with $Z = 39$, correspond to the middle of the proton major shell $Z = 28$–50, and their even-even boson cores are here considered to be Sr nuclei ($Z = 38$). Alternatively, one may also consider Zr cores for Y.

(iii) The parameters Γ_ρ, Λ_ρ, and A_ρ, which are determined by fitting to the neighboring odd-N and odd-Z nuclei, are used for the odd-odd nucleus. The quasiparticle energies, $\tilde{\epsilon}_{j_\rho}$, and occupation probabilities, $v^2_{j_\rho}$, are newly calculated. Then the interaction strengths in the fermion-fermion interaction (8) are fixed to reproduce, to a certain accuracy, the observed low-lying positive-parity levels of each odd-odd nucleus.

TABLE I. The even-even core, neighboring odd-N, odd-Z, and odd-odd nuclei with the neutron number $N = 54$–64 considered in the present study.

Even-even	Odd-N	Odd-Z	Odd-odd
${}_{48}\mathrm{Cd}_N$	${}_{48}\mathrm{Cd}_{N+1}$	${}_{47}\mathrm{Ag}_N$	${}_{47}\mathrm{Ag}_{N+1}$
${}_{46}\mathrm{Pd}_N$	${}_{46}\mathrm{Pd}_{N+1}$	${}_{45}\mathrm{Rh}_N$	${}_{45}\mathrm{Rh}_{N+1}$
${}_{44}\mathrm{Ru}_N$	${}_{44}\mathrm{Ru}_{N+1}$	${}_{43}\mathrm{Tc}_N$	${}_{43}\mathrm{Tc}_{N+1}$
${}_{42}\mathrm{Mo}_N$	${}_{42}\mathrm{Mo}_{N+1}$	${}_{41}\mathrm{Nb}_N$	${}_{41}\mathrm{Nb}_{N+1}$
${}_{40}\mathrm{Zr}_N$	${}_{40}\mathrm{Zr}_{N+1}$	–	–
${}_{38}\mathrm{Sr}_N$	${}_{38}\mathrm{Sr}_{N+1}$	${}_{39}\mathrm{Y}_{N+1}$	${}_{39}\mathrm{Y}_{N+1}$
${}_{36}\mathrm{Kr}_N$	${}_{36}\mathrm{Kr}_{N+1}$	${}_{37}\mathrm{Rb}_{N+1}$	${}_{37}\mathrm{Rb}_{N+1}$

The IBFFM-2 Hamiltonian, with the parameters determined by the above procedure, is diagonalized to yield excitation energies and wave functions of the odd-odd systems.

D. Electromagnetic transition operators

By using the IBFFM-2 wave functions, electromagnetic properties are calculated. The $E2$ operator is defined as

$$\hat{T}^{(E2)} = \hat{T}^{(E2)}_{\rm B} + \hat{T}^{(E2)}_{\rm F}, \tag{11}$$

with the boson part,

$$\hat{T}^{(E2)}_{\rm B} = e^{\rm B}_\nu\hat{Q}_\nu + e^{\rm B}_\pi\hat{Q}_\pi, \tag{12}$$

and the fermion part,

$$\hat{T}^{(E2)}_{\rm F} = -\frac{1}{\sqrt{5}}\sum_{\rho=\nu,\pi}\sum_{j_\rho j'_\rho}\left(u_{j_\rho}u_{j'_\rho} - v_{j_\rho}v_{j'_\rho}\right) \times \left\langle \ell_\rho\frac{1}{2}j_\rho\middle\| e^{\rm F}_\rho r^2 Y^{(2)}\middle\|\ell'_\rho\frac{1}{2}j'_\rho\right\rangle\left(a^\dagger_{j_\rho}\times\tilde{a}_{j'_\rho}\right)^{(2)}. \tag{13}$$

$e^{\rm B}_\rho$ are the boson effective charges, and the common values for the neutrons and protons, i.e., $e^{\rm B}_\nu = e^{\rm B}_\pi = 0.0577$ eb, which

were used in the previous IBFFM-2 calculations for the Ge and As nuclei [54], are employed here. The neutron and proton effective charges, $e_\nu^{\rm F} = 0.5\ e$b and $e_\pi^{\rm F} = 1.5\ e$b, are exploited also from Ref. [54]. The $M1$ transition operator $\hat{T}^{(M1)}$ reads

$$\hat{T}^{(M1)} = \sqrt{\frac{3}{4\pi}} \sum_{\rho=\nu,\pi} \Bigg[g_\rho^{\rm B} \hat{L}_\rho - \frac{1}{\sqrt{3}} \sum_{j_\rho j'_\rho} \left(u_{j_\rho} u_{j'_\rho} + v_{j_\rho} v_{j'_\rho}\right) \times \langle j_\rho \| g_l^\rho \ell + g_s^\rho \mathbf{s} \| j'_\rho \rangle \left(a^\dagger_{j_\rho} \times \tilde{a}_{j'_\rho}\right)^{(1)} \Bigg]. \tag{14}$$

The empirical g factors for the neutron and proton bosons, $g_\nu^{\rm B} = 0\,\mu_N$ and $g_\pi^{\rm B} = 1.0\,\mu_N$, respectively, are adopted. For the neutron (or proton) g factors, the free values $g_\ell^\nu = 0\,\mu_N$ and $g_s^\nu = -3.82\,\mu_N$ ($g_\ell^\pi = 1.0\,\mu_N$ and $g_s^\pi = 5.58\,\mu_N$) are employed, with g_s^ρ quenched by 30% as is the case of many of the realistic IBFFM-2 calculations (e.g., Ref. [25]).

E. Gamow-Teller transition operator

To study β-decay properties, Gamow-Teller (GT) transition strengths are computed. Here, the Fermi transitions do not enter the β decay of the studied nuclei, since the single-particle space considered for the odd-odd nuclei consists of the neutron $3s_{1/2}$, $2d_{3/2}$, $2d_{5/2}$, and $1g_{7/2}$ orbitals, and the proton $1g_{9/2}$ orbital, and there is no coupling between these single-particle orbitals to the angular momentum zero that gives rise to the Fermi transition.

The GT transition operator is here defined by

$$\hat{T}^{\rm GT} = \sum_{j_\nu j_\pi} \eta^{\rm GT}_{j_\nu j_\pi} \left(\hat{P}_{j_\nu} \times \hat{P}_{j_\pi}\right)^{(1)}, \tag{15}$$

with the coefficients η calculated as

$$\eta^{\rm GT}_{j_\nu j_\pi} = -\frac{1}{\sqrt{3}} \left\langle \ell_\nu \frac{1}{2} j_\nu \middle\| \boldsymbol{\sigma} \middle\| \ell_\pi \frac{1}{2} j_\pi \right\rangle \delta_{\ell_\nu \ell_\pi}. \tag{16}$$

$\hat{P}_{j_\rho}$ in Eq. (15) is a one-particle transfer operator, expressed as one of these operators,

$$A^\dagger_{j_\rho m_\rho} = \zeta_{j_\rho} a^\dagger_{j_\rho m_\rho} + \sum_{j'_\rho} \zeta_{j_\rho j'_\rho} s^\dagger_\rho \left(\tilde{d}_\rho \times a^\dagger_{j'_\rho}\right)^{(j_\rho)}_{m_\rho}, \tag{17}$$

$$B^\dagger_{j_\rho m_\rho} = \theta_{j_\rho} s^\dagger_\rho \tilde{a}_{j_\rho m_\rho} + \sum_{j'_\rho} \theta_{j_\rho j'_\rho} \left(d^\dagger_\rho \times \tilde{a}_{j'_\rho}\right)^{(j_\rho)}_{m_\rho}, \tag{18}$$

which increases the number of valence nucleons, $2N_\rho + n_{j_\rho}$, by 1, and their conjugate operators,

$$\tilde{A}_{j_\rho m_\rho} = \zeta^*_{j_\rho} \tilde{a}_{j_\rho m_\rho} + \sum_{j'_\rho} \zeta^*_{j_\rho j'_\rho} s_\rho \left(d^\dagger_\rho \times \tilde{a}_{j'_\rho}\right)^{(j_\rho)}_{m_\rho}, \tag{19}$$

$$\tilde{B}_{j_\rho m_\rho} = -\theta^*_{j_\rho} s_\rho a^\dagger_{j_\rho m_\rho} - \sum_{j'_\rho} \theta^*_{j_\rho j'_\rho} \left(\tilde{d}_\rho \times a^\dagger_{j'_\rho}\right)^{(j_\rho)}_{m_\rho}, \tag{20}$$

which decreases the valence nucleon number by 1. In addition, the operators in Eqs. (17) and (18) [Eqs. (19) and (20)], respectively, increase and decrease the number of like-particle (like-hole) nucleons. The $\hat{T}^{\rm GT}$ operator can be constructed by using two of those operators defined in Eqs. (17)–(20), depending on the type of the β decay under study (i.e., β^+ or β^-), and on the particle or hole nature of bosons in the even-even IBM-2 core. To be more specific, for the β^- decay, $\hat{P}_{j_\nu} = \tilde{A}_{j_\nu m_\nu}$ and $\hat{P}_{j_\pi} = \tilde{B}_{j_\pi m_\pi}$ for those nuclei with $Z \geqslant 39$, and $\hat{P}_{j_\nu} = \tilde{A}_{j_\nu m_\nu}$ and $\hat{P}_{j_\pi} = \tilde{A}^\dagger_{j_\pi m_\pi}$ for $Z \leqslant 38$. Their conjugate operators correspond to those describing the β^+ decay or electron-capture (EC) process.

The coefficients ζ_j, $\zeta_{jj'}$, θ_j, and $\theta_{jj'}$ in Eqs. (17)–(20) are calculated by the following formulas obtained within the generalized seniority scheme [72]:

$$\zeta_{j_\rho} = u_{j_\rho} \frac{1}{K'_{j_\rho}}, \tag{21a}$$

$$\zeta_{j_\rho j'_\rho} = -v_{j_\rho} \beta_{j'_\rho j_\rho} \sqrt{\frac{10}{N_\rho (2j_\rho + 1)}} \frac{1}{K K'_{j_\rho}}, \tag{21b}$$

$$\theta_{j_\rho} = \frac{v_{j_\rho}}{\sqrt{N_\rho}} \frac{1}{K''_{j_\rho}}, \tag{21c}$$

$$\theta_{j_\rho j'_\rho} = u_{j_\rho} \beta_{j'_\rho j_\rho} \sqrt{\frac{10}{2j_\rho + 1}} \frac{1}{K K''_{j_\rho}}. \tag{21d}$$

The factors K, K'_{j_ρ}, and K''_{j_ρ} read

$$K = \left(\sum_{j_\rho j'_\rho} \beta^2_{j_\rho j'_\rho} \right)^{1/2}, \tag{22a}$$

$$K'_{j_\rho} = \left[1 + 2 \left(\frac{v_{j_\rho}}{u_{j_\rho}} \right)^2 \frac{\left\langle (\hat{n}_{s_\rho} + 1) \hat{n}_{d_\rho} \right\rangle_{0_1^+}}{N_\rho (2j_\rho + 1)} \frac{\sum_{j'_\rho} \beta^2_{j'_\rho j_\rho}}{K^2} \right]^{1/2}, \tag{22b}$$

$$K''_{j_\rho} = \left[\frac{\langle \hat{n}_{s_\rho} \rangle_{0_1^+}}{N_\rho} + 2 \left(\frac{u_{j_\rho}}{v_{j_\rho}} \right)^2 \frac{\left\langle \hat{n}_{d_\rho} \right\rangle_{0_1^+}}{2j_\rho + 1} \frac{\sum_{j'_\rho} \beta^2_{j'_\rho j_\rho}}{K^2} \right]^{1/2}, \tag{22c}$$

where $\hat{n}_{s_\rho}$ is the number operator for the s_ρ boson and $\langle \cdots \rangle_{0_1^+}$ represents the expectation value in the ground state of the even-even core. The occupation, v_{j_ρ}, and unoccupation, u_{j_ρ}, amplitudes in the above expressions are the same as those used when constructing the IBFFM-2 Hamiltonian.

It is noted that the operator, $\hat{P}_{j_\rho}$, adopted in the present study is of a specific form, as it depends only on the amplitudes v_{j_ρ} and u_{j_ρ}. One could consider more complicated one-particle transfer operators that are parametrized in some different ways or that include some higher-order terms, especially because the final results on the β-decay properties are supposed to be influenced by the form of the operator. Such a more general form of the transfer operator would also involve additional parameters that are needed for a better description of the experimental data, which, in turn, could cause further complications and theoretical uncertainties. The use of the simplified operators in Eqs. (17)–(20), specified by the v_{j_ρ} and u_{j_ρ} amplitudes only, has an advantage of not having to introduce any phenomenological parameter in the calculation of β decay.

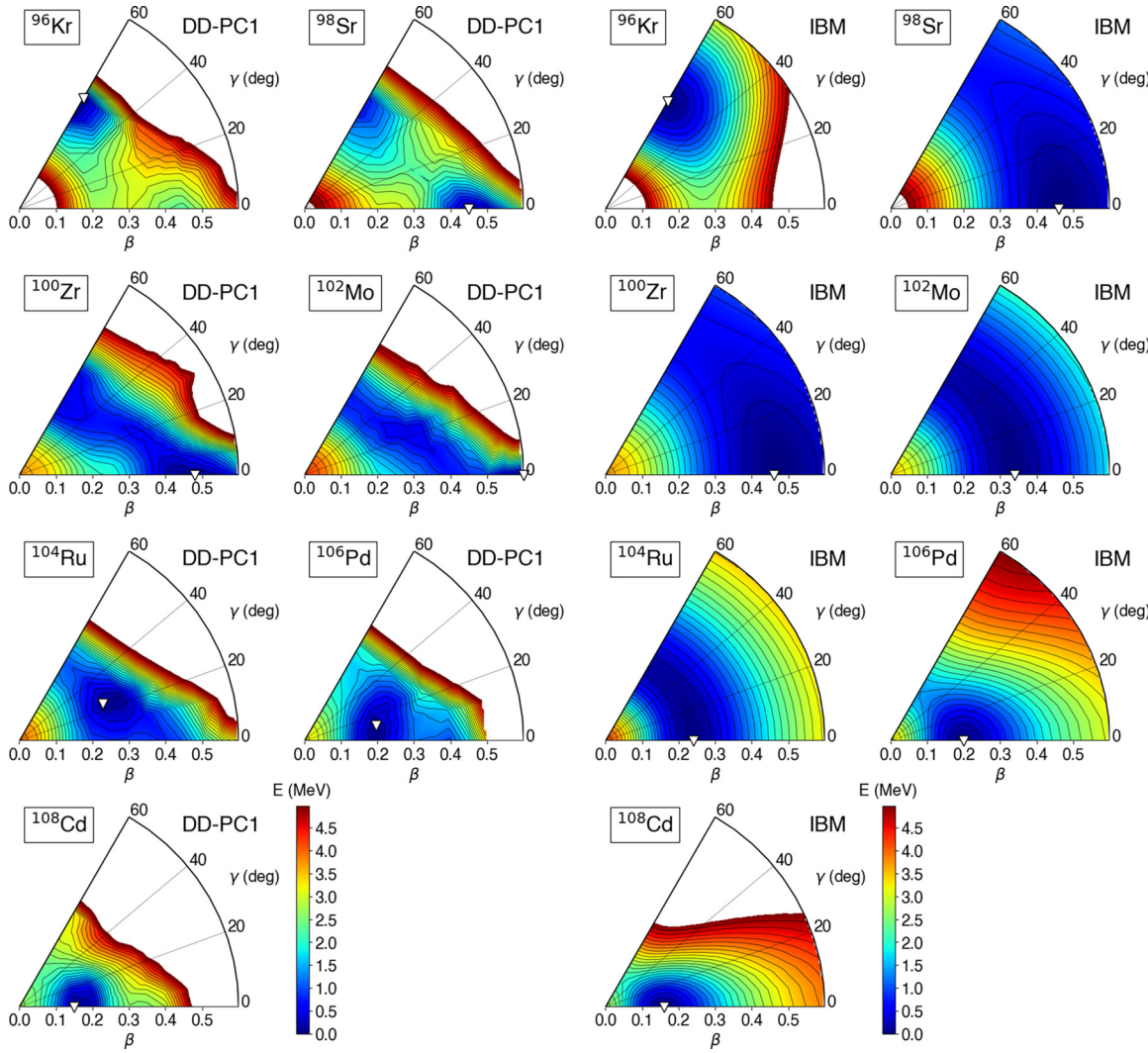

FIG. 1. Columns 1 and 2: Contour plots of the triaxial quadrupole (β, γ) PESs for the even-even $N = 60$ isotones calculated within the constrained relativistic Hartree-Bogoliubov method employing the energy functional DD-PC1 and separable pairing force of finite range. Columns 3 and 4: The corresponding mapped PESs in the IBM-2. The global minimum is indicated by an open triangle, and the difference between the neighboring contours is 0.2 MeV.

III. LOW-LYING STRUCTURE OF THE INITIAL AND FINAL NUCLEI

A. Potential energy surfaces

In the first and second columns of Fig. 1 the triaxial quadrupole (β, γ) PESs for the $N = 60$ isotones, from ^{96}Kr to ^{108}Cd, computed within the constrained RHB method with the DD-PC1 EDF and a separable pairing force, are shown. For ^{96}Kr and ^{98}Sr the SCMF calculation predicts two minima on the oblate and prolate sides of the PESs. The energy surfaces for ^{100}Zr, ^{102}Mo, and ^{104}Ru are particularly soft in γ deformation. For ^{104}Ru a triaxial minimum around $\gamma \approx 30^\circ$ is found. The nuclei ^{106}Pd and ^{108}Cd are suggested to be more weakly (prolate) deformed, as expected from the fact that they are rather close to the proton $Z = 50$ major shell closure.

The SCMF PESs can be compared with the mapped IBM-2 PESs, which are shown in the third and fourth columns of Fig. 1. One could observe certain similarities between the IBM-2 and SCMF PESs, in that basic characteristics of the latter in the neighborhood of the global minimum are reproduced in the former. The difference between the SCMF and IBM-2 PESs becomes visible for those configurations that correspond to large β deformation, so that the IBM-2 surface is flat as compared to the SCMF one. This is due to the restricted degrees of freedom in the IBM-2 framework; that is, the IBM-2 is built only on the valence nucleons in one major oscillator shell while the SCMF model comprises all nucleons.

Another notable difference between the SCMF and IBM-2 PESs is that the former exhibits several minima that are close in energy to each other, most spectacularly in ^{96}Kr and ^{98}Sr, whereas a single minimum is found in the IBM-2 PES in both cases. Here it is assumed that low-lying states in the vicinity of the ground state are determined mainly by the configurations near the absolute minimum of the SCMF PES, and hence the mapping is carried out so as to reproduce the topology of

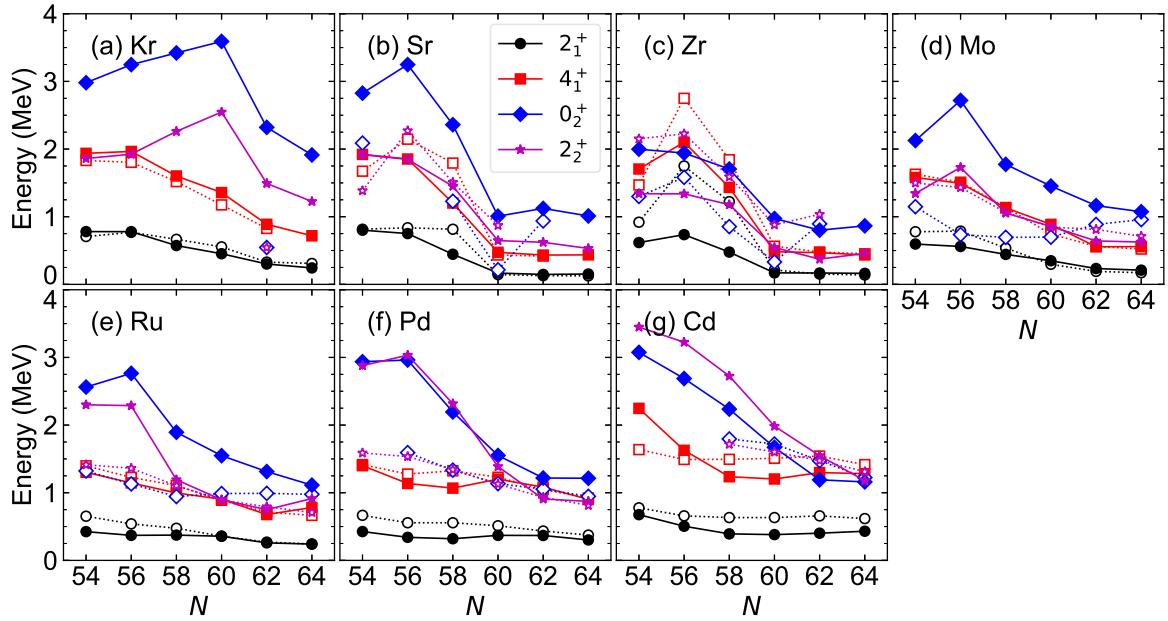

FIG. 2. Calculated excitation spectra of the 2_1^+, 4_1^+, 0_2^+, and 2_2^+ states of the even-even Kr, Sr, Zr, Mo, Ru, Pd, and Cd isotopes (solid symbols connected by solid lines). The experimental data (open symbols connected by dotted lines) are adopted from the NNDC database [73].

only that region of the SCMF PES. This assumption may not hold for those nuclei for which multiple mean-field minima are found. Particularly in ^{98}Sr, even though the oblate and prolate mean-field minima differ in energy only by 0.67 MeV, the mapping is carried out only to reproduce the prolate global minimum at $\beta = 0.45$. The IBM-2 Hamiltonian for ^{98}Sr could be constructed based on the oblate secondary minimum at $\beta = 0.3$. In that case the nature of the wave function would be considerably different from otherwise, and this would severely affect the β-decay properties. It should be also noted that the oblate-prolate balance in the energy surface is so subtle that it depends on the nuclear EDF that underlies the IBM-2 calculation. These possibilities should be thoroughly investigated in future.

There is, nevertheless, a way of producing the multiple minima on the energy surface within the IBM-2, that is, by the inclusion of the configuration mixing between several different boson spaces differing in boson number by two [74]. Alternatively, cubic, or three-body, boson terms with negative strength parameter could be introduced in the IBM-2 Hamiltonian [15], which are also expected to produce two minima on the prolate and oblate sides. These extensions are, however, not attempted in the present work, mainly because both the configuration mixing and the inclusion of the cubic terms cannot be handled with the current version of the IBFFM-2 code.

Furthermore, as noted earlier, the SCMF PES for ^{104}Ru exhibits a triaxial minimum at $\gamma \approx 30^\circ$, while the IBM-2 one does not. This discrepancy could be solved by including the three-body boson terms with a positive strength parameter [51]. By the inclusion of these terms, the observed level structure and $E2$ transition properties of the γ-vibrational bands of γ-soft nuclei are shown [51] to be better reproduced, but the energy levels of the ground-state and excited 0^+ bands are not altered significantly. For this reason, and since in the following discussion mainly the β decay that involves the 0_1^+ ground states of the even-even nuclei is considered, the three-body boson terms are neglected in the present calculation. In some cases, however, the triaxiality could make non-negligible contributions to the nuclear wave functions, and it will be of great interest to investigate the roles played by the quadrupole triaxiality in the β-decay properties.

B. IBM-2 results for the even-even nuclei

Figure 2 depicts the excitation energies of the 2_1^+, 4_1^+, 0_2^+, and 2_2^+ states of the even-even Kr, Sr, Zr, Mo, Ru, Pd, and Cd nuclei with $54 \leqslant N \leqslant 64$ calculated with the mapped IBM-2. Note that the results for the Zr isotopes have already been presented in Ref. [15], but they are included in the plot for the sake of completeness. One could observe in Fig. 2 that the mapped IBM-2 gives a reasonable description of the observed 2_1^+ and 4_1^+ excitation energies for all the isotopic chains, except for the Zr one. In many cases, the 0_2^+ and 2_2^+ energy levels are overestimated for nearly spherical nuclei that are close to the $N = 50$ magic number, for which the IBM description in general becomes less reliable. For the Sr and Zr isotopes, the calculated low-lying levels exhibit a rapid decrease in energy starting from $N = 56$ to 60. This behavior of the levels can be interpreted as a signature of the shape phase transition from the nearly spherical to deformed configurations. The high-lying 2_1^+ energy level observed for ^{96}Zr is due to the filling of the neutron $d_{5/2}$ subshell closure. As addressed in Ref. [15], the major reason why the mapped IBM-2 is not able to reproduce the level structure of the Zr isotopes in the transitional regions, i.e., $N = 56$ and 58, is that the RHB PESs for these nuclei suggest strong deformation and the resultant IBM-2 energy levels are rather compressed.

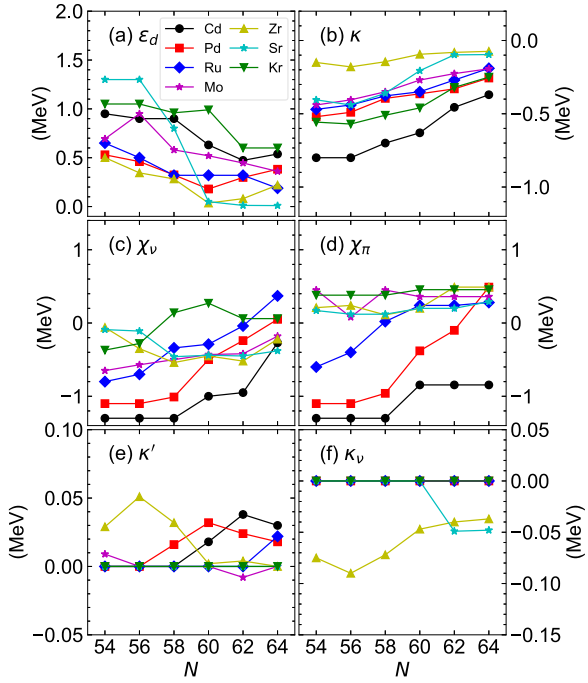

FIG. 3. Adopted strength parameters of the IBM-2 Hamiltonian for the even-even nuclei studied in the present work.

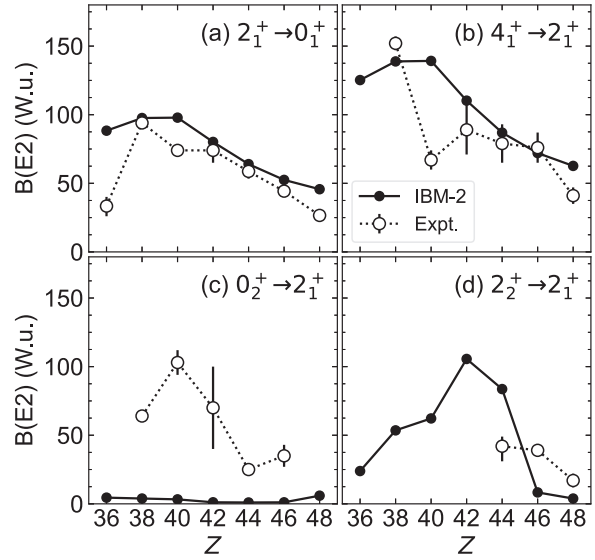

FIG. 4. Calculated and experimental [73] (a) $B(E2; 2_1^+ \to 0_1^+)$, (b) $B(E2; 4_1^+ \to 2_1^+)$, (c) $B(E2; 0_2^+ \to 2_1^+)$, and (d) $B(E2; 2_2^+ \to 2_1^+)$ transition strengths for the even-even $N = 60$ isotones as functions of the proton number Z.

In many of the previous mapped IBM-2 calculations, the 0_2^+ excitation energies have been quite often overestimated. Such a problem could be explained in part by the fact that the underlying EDF calculation generally suggests a too large deformation and one has to choose the quadrupole-quadrupole interaction strength κ that is unexpectedly larger in magnitude than those which have been often used in phenomenological IBM-2 fitting calculations.

Figure 3 shows evolution of the derived IBM-2 parameters as functions of N employed in the present calculation. One can find some correlations between the behaviors of the low-lying levels and those of the IBM-2 parameters. In Fig. 3(a), for instance, the decrease with N of the single d boson energy, ϵ_d, indicates development of quadrupole deformation. The decrease in magnitude of the parameter κ with N is also a signature of increasing quadrupole collectivity [Fig. 3(b)]. The average of the parameters, $\chi \equiv (\chi_\nu + \chi_\pi)/2$, and its sign reflect whether the nucleus is prolate ($\chi < 0$) or oblate ($\chi > 0$) deformed in the SCMF calculations. For many of the nuclei, particularly in the Kr, Sr, Zr, and Mo isotopes, the average χ is close to zero, indicating the γ softness that is found in the corresponding PESs (see, Fig. 1). The $\hat{L} \cdot \hat{L}$ term is considered only for those nuclei for which the IB moment of inertia is calculated to be appreciable, i.e., approximately larger than 10. Otherwise, the strength parameter of this term is simply set as $\kappa' = 0$.

Figure 4 shows the calculated $B(E2)$ values in Weisskopf units (W.u.) for the even-even $N = 60$ isotones. The mapped IBM-2 provides overall a reasonable quantitative and qualitative description of the $B(E2; 2_1^+ \to 0_1^+)$ [Fig. 4(a)] and $B(E2; 4_1^+ \to 2_1^+)$ [Fig. 4(b)] transition strengths, even though the common boson effective charges are used for all the nuclei considered. An exception is perhaps the $B(E2; 4_1^+ \to 2_1^+)$ value for ^{100}Zr, for which the IBM-2 gives twice as large as that of the experimental data. However, the observed $B(E2; 4_1^+ \to 2_1^+)$ value is 67 ± 7 W.u., which is smaller than, or in the same order of magnitude as, the $B(E2; 2_1^+ \to 0_1^+)$ value of 74 ± 4 W.u. This systematic would not be reproduced within the present IBM-2 model space consisting of a single configuration, giving rise to only the $B(E2; 4_1^+ \to 2_1^+)$ rate that is greater than the $B(E2; 2_1^+ \to 0_1^+)$ one.

As seen from Fig. 4(c) the observed $B(E2; 0_2^+ \to 2_1^+)$ rates of the $N = 60$ isotones are generally large, that is, of the orders of >20 W.u. The large $B(E2; 0_2^+ \to 2_1^+)$ values are often considered a signature of strong shape mixing or shape coexistence. Particularly large $B(E2; 0_2^+ \to 2_1^+)$ values of >60 W.u. that are found experimentally for the ^{98}Sr, ^{100}Zr, and ^{102}Mo are considered to be a consequence of strong shape mixing in these nuclei. On the contrary, the mapped IBM-2 suggests too small $B(E2; 0_2^+ \to 2_1^+)$ values for all the $N = 60$ isotones. The vanishing $B(E2; 0_2^+ \to 2_1^+)$ rate implies that the mixing between the ground state and the 0_2^+ states is not properly accounted for in the present calculation. A possible remedy for this inconsistency would be to include in the IBM-2 the configuration mixing, since this extension often works in reproducing strong $B(E2; 0_2^+ \to 2_1^+)$ rates for those nuclei where shape coexistence is suggested to occur. Another major cause of the inconsistency could be attributed to the SCMF PESs calculated for these $N = 60$ isotones, which generally suggest a too strong deformation. As a consequence, the mapped IBM-2 ends up giving a more rotational structure than expected, exhibiting a weak $0_2^+ \to 2_1^+$ transition.

As one sees in Fig. 4(d), enhanced $B(E2; 2_2^+ \to 2_1^+)$ transition rates are predicted in the mapped IBM-2 calculation. This transition is often considered an indicator of the γ softness,

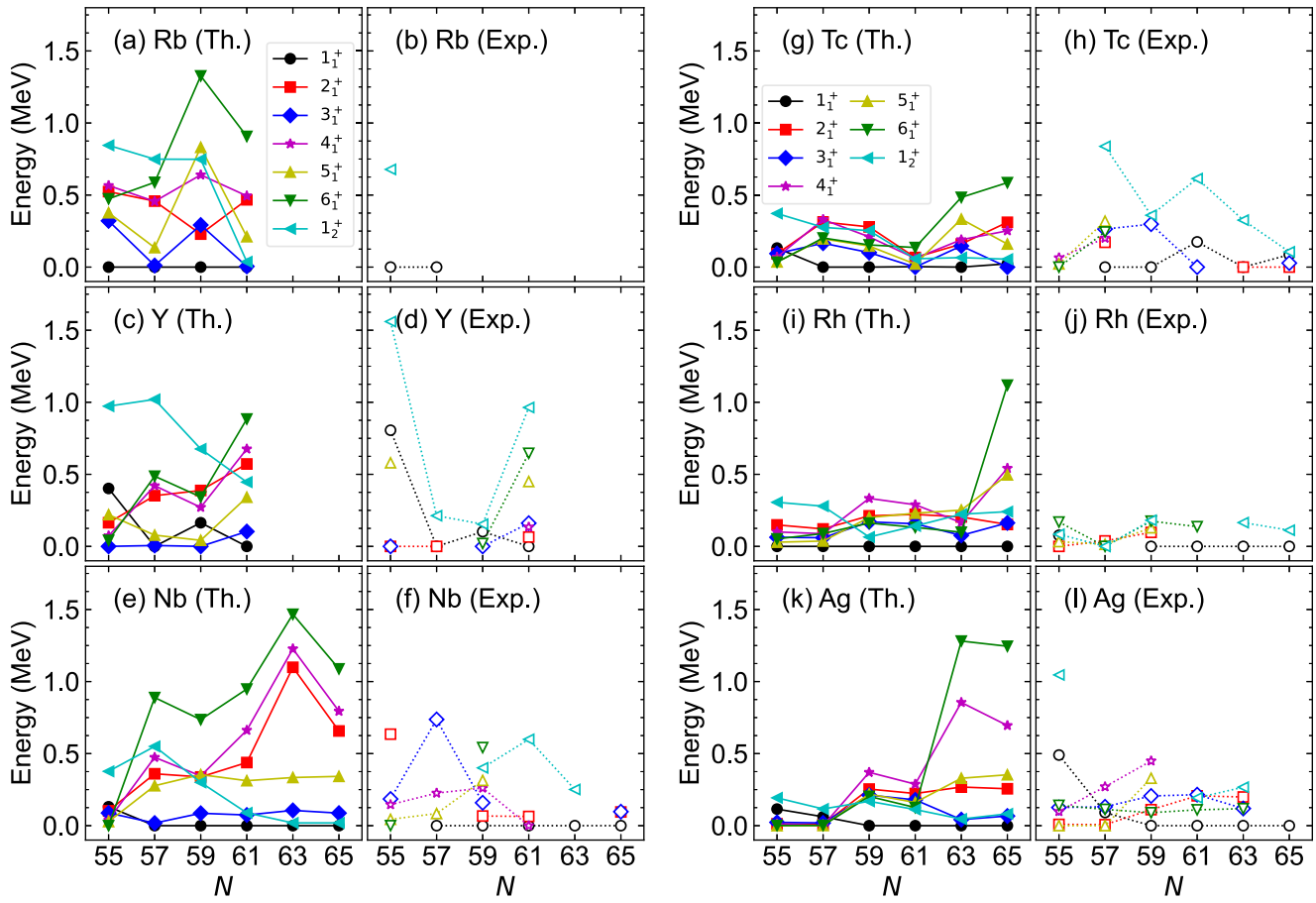

FIG. 5. Calculated and experimental excitation energies of the low-spin positive-parity states of the odd-odd nuclei.

which is indeed shown to be most significant around ^{102}Mo and ^{104}Ru in the corresponding SCMF PESs (see Fig. 1).

C. IBFFM-2 results for the odd-odd nuclei

The calculated excitation spectra of the low-lying positive-parity states of the odd-odd Rb, Y, Nb, Tc, Rh, and Ag nuclei are presented in Fig. 5, in comparison with the available experimental data [73]. For Rb and Y isotopes calculations are made only for those nuclei for which experimental information is available or the same strength parameters of the IBFFM-2 Hamiltonian as those fitted to the available data on neighboring nuclei are used (for Rb). Theoretical excitation energies for ^{100}Rb and ^{102}Rb are therefore not shown in the figure. Calculated energies are also not shown for ^{102}Y and ^{104}Y, which is because the present version of the IBFFM-2 code is unable to handle the dimension of the IBFFM-2 Hamiltonian matrices for these nuclei.

One observes, in Fig. 5, rapid evolution of energy levels at particular isotopes within the range $N = 57$–61, which is in many cases accompanied by the change of the ground-state spin. The structural evolution is most clearly seen, both theoretically and experimentally, in the Y isotopic chain, and reflects the shape phase transition at $N \approx 60$ in the even-even boson Sr core [see Fig. 2(b)]. For the Nb, Tc, Rh, and Ag isotopic chains, the majority of the isotopes with $N \geqslant 59$ have the 1^+ state as the lowest-energy positive-parity state, while near the neutron shell closure $N = 50$ those states with spin higher than 1^+ become the ground state.

Table II lists the adopted strength parameters for the IBFFM-2 Hamiltonian, i.e., those for the boson-fermion interactions (Γ_ν, Γ_π, Λ_ν, Λ_π, A_ν, and A_π) and for the residual fermion-fermion interactions. In the present calculations, the δ-type and tensor interactions turn out to be most important to reproduce the low-energy spectra of odd-odd nuclei. Fixed values are used for the strength parameter for the δ term, $v_\mathrm{d} = -0.08$ MeV, and that for the spin-spin-δ term is set to zero, $v_\mathrm{ssd} = 0$ MeV. The spin-spin term is also assumed to be zero, but is introduced specifically for the ^{98}Tc and ^{96}Nb nuclei, with the corresponding strengths being $v_\mathrm{ss} = 0.1$ MeV for both nuclei, in order to reproduce the ground-state spin of 6^+. The energy of the 1^+ states turns out to be quite sensitive to the tensor interaction strength, v_t. As seen in Table II, the adopted v_t strength indeed varies from one nucleus to another, so that the 1^+ state should be the ground state in many of the nuclei.

Figure 6 exhibits fractions of the pair components denoted $[\nu s_{1/2} \otimes \pi g_{9/2}]^{(J)}$, $[\nu d_{3/2} \otimes \pi g_{9/2}]^{(J)}$, $[\nu d_{5/2} \otimes \pi g_{9/2}]^{(J)}$, and $[\nu g_{7/2} \otimes \pi g_{9/2}]^{(J)}$ in the wave functions of the 1_1^+ state of the odd-odd nuclei. In most of the cases shown in the figure, the

TABLE II. Adopted strength parameters (in MeV units) for the boson-fermion interactions, and fermion-fermion interactions in the IBFFM-2 Hamiltonian describing the considered odd-odd nuclei. The fixed values, $v_{\rm d} = -0.08$ MeV, $v_{\rm ssd} = 0.0$ MeV, are employed for the δ and spin-spin-δ terms, respectively. The spin-spin interaction strength, $v_{\rm ss}$, is chosen to be zero for all nuclei, but for $v_{\rm ss} = 0.1$ MeV for ^{98}Tc and ^{96}Nb.

Nucleus	Γ_ν	Γ_π	Λ_ν	Λ_π	A_ν	A_π	$v_{\rm t}$
^{102}Ag	0.30	0.30	0.70	1.70	−0.50	−2.00	0.000
^{104}Ag	0.30	0.30	0.70	1.70	−0.20	−0.70	0.000
^{106}Ag	0.30	0.30	0.70	1.40	−0.00	−0.70	0.060
^{108}Ag	0.30	0.30	0.70	1.30	−0.00	−0.00	0.055
^{110}Ag	0.10	0.30	3.00	1.30	−0.20	−0.80	0.500
^{112}Ag	0.10	0.30	2.60	1.00	−0.30	−0.00	0.700
^{100}Rh	0.30	0.30	0.60	1.00	−0.00	−0.80	0.030
^{102}Rh	0.30	0.30	0.20	0.35	−0.00	−0.00	0.020
^{104}Rh	0.30	0.30	0.20	1.00	−0.00	−0.80	0.055
^{106}Rh	0.30	0.30	0.00	1.20	−0.00	−0.00	0.050
^{108}Rh	1.50	0.30	0.70	1.00	−0.20	−0.40	0.050
^{110}Rh	1.50	0.30	0.10	1.00	−0.50	−0.50	0.400
^{98}Tc	0.30	0.30	0.40	0.70	−0.00	−0.00	0.000
^{100}Tc	0.30	0.30	0.35	0.90	−0.00	−0.00	0.050
^{102}Tc	0.30	0.30	0.44	0.70	−0.00	−0.00	0.040
^{104}Tc	0.30	0.30	0.60	2.60	−0.40	−3.00	0.030
^{106}Tc	0.30	0.30	0.30	2.10	−0.00	−3.00	0.150
^{108}Tc	0.30	0.10	0.90	2.20	−1.20	−0.00	0.500
^{96}Nb	0.30	0.30	0.40	0.90	−0.00	−0.50	−0.000
^{98}Nb	1.50	0.10	0.80	0.00	−1.20	−0.00	0.280
^{100}Nb	1.50	0.30	0.50	0.20	−1.40	−0.80	0.500
^{102}Nb	1.50	0.10	0.90	3.80	−0.90	−2.00	0.500
^{104}Nb	1.50	0.10	1.55	3.80	−0.90	−2.00	0.800
^{106}Nb	1.50	0.10	1.00	3.80	−0.30	−2.00	0.800
^{94}Y	0.10	1.00	0.40	0.00	−1.00	−0.40	0.000
^{96}Y	0.50	1.00	0.10	0.00	−0.00	−0.50	0.060
^{98}Y	0.50	1.00	0.10	0.00	−0.00	−0.00	0.040
^{100}Y	0.50	0.50	0.80	12.00	−0.80	−0.00	2.000
^{92}Rb	0.30	0.50	0.40	0.00	−1.00	−0.30	0.080
^{94}Rb	0.70	0.50	0.20	0.00	−2.00	−1.00	0.100
^{96}Rb	0.70	0.50	0.00	0.00	−0.00	−2.00	0.500
^{98}Rb	0.30	0.10	2.20	34.00	−5.00	−5.00	0.500

configuration of the $[\nu g_{7/2} \otimes \pi g_{9/2}]^{(J)}$ pairs coupled to the even-even boson cores predominates the 1_1^+ wave functions typically for those nuclei with the neutron numbers $N \leqslant 59$. For heavier isotopes with N larger than 59, other pair components start to play a role, especially the $[\nu d_{3/2} \otimes \pi g_{9/2}]^{(J)}$ ones. The $[\nu s_{1/2} \otimes \pi g_{9/2}]^{(J)}$ pairs do not appear to play an important role in the 1_1^+ state of all the nuclei considered. The change in the composition of the wave function for the odd-odd nuclei reflects the shape phase transitions in the even-even core nuclei and, as shown later, influences the predicted systematic of β-decay properties.

Table III compares the calculated and experimental $B(E2)$ and $B(M1)$ transition rates, and electric quadrupole $Q(I)$ and magnetic dipole $\mu(I)$ moments. One notices that the present IBFFM-2 generally gives a reasonable description of the $Q(I)$ and $\mu(I)$ moments including sign. Limited experimental data are available to compare for the $B(E2)$ and $B(M1)$ transition

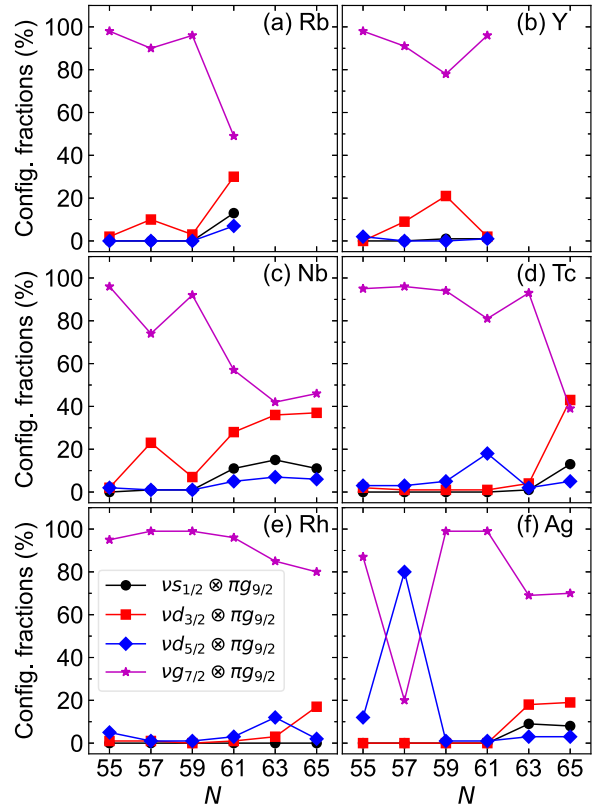

FIG. 6. Fractions in percent of the configurations in terms of the pair components $[\nu s_{1/2} \otimes \pi g_{9/2}]^{(J)}$, $[\nu d_{3/2} \otimes \pi g_{9/2}]^{(J)}$, $[\nu d_{5/2} \otimes \pi g_{9/2}]^{(J)}$, and $[\nu g_{7/2} \otimes \pi g_{9/2}]^{(J)}$ that are coupled to even-even boson cores in the IBFFM-2 wave function of the 1_1^+ state for the studied odd-odd nuclei.

rates. Some deviations are present between the calculated and experimental data for the transition rates, which could be understood in terms of the different nature of the IBFFM-2 wave functions for the initial and final states. In ^{102}Ag, for example, the present IBFFM-2 calculation underestimates the observed $B(E2)$ rates, but overestimates the $B(M1)$ ones. The dominant pair component in the 5_1^+ ground state for ^{102}Ag is here suggested to be of the type $[\nu d_{5/2} \otimes \pi g_{9/2}]^{(J=5)}$, which accounts for 95% of the corresponding wave function. On the other hand, the 6_1^+ state for the same nucleus is suggested to be dominated by the $[\nu d_{5/2} \otimes \pi g_{9/2}]^{(J=6)}$ (87%) and $[\nu d_{5/2} \otimes \pi g_{9/2}]^{(J=7)}$ (10%) pair components. For both the $E2$ and $M1 6_1^+ \to 5_1^+$ transitions, the fermionic part of the transition operators, $\hat{T}_{\rm F}^{(E2/M1)}$ [Eqs. (11) and (14)], are found to make major contributions to the transition matrix elements. The fermion contribution seems to be less significant in the $E2$ matrix element, but makes a substantial contribution to the $M1$ matrix element. These observations may help in understanding the deviations in the transition properties shown in Table III.

In general, however, the experimental information about the electromagnetic transitions is still so scarce in the odd-odd nuclei in the considered mass region that it is rather hard to draw a concrete conclusion about the performance of the IBFFM-2 in computing these observables.

TABLE III. Comparison of the calculated and experimental [73,75] $B(E2)$ (in W.u.) and $B(M1)$ (in μ_N^2) transitions, $Q(I)$ (in eb), and $\mu(I)$ (in μ_N) moments for the odd-odd nuclei considered in this study.

Nucleus	Property	IBFFM-2	Experiment
^{96}Rb	$\mu(2_1^+)$	2.42	$+1.466 \pm 0.002$
	$Q(2_1^+)$	0.48	$+0.25 \pm 0.06$
^{96}Nb	$\mu(6_1^+)$	4.71	4.976 ± 0.004
^{100}Nb	$B(M1; 1_2^+ \to 1_1^+)$	0.25	$0.0038^{+0.0019}_{-0.0010}$
^{102}Ag	$B(E2; 6_1^+ \to 5_1^+)$	0.64	32 ± 16
	$B(M1; 6_1^+ \to 5_1^+)$	1.18	0.0011 ± 0.0004
	$\mu(5_1^+)$	4.38	$+4.6 \pm 0.7$
	$\mu(2_1^+)$	5.43	$+4.1 \pm 0.3$
	$\mu(7_1^+)$	4.52	4.6 ± 0.3
^{104}Ag	$B(M1; 6_1^+ \to 5_1^+)$	0.12	>0.0089
	$B(M1; 7_1^+ \to 6_1^+)$	0.03	0.0085 ± 0.0020
	$B(E2; 7_1^+ \to 6_1^+)$	28.96	$(1.2 \pm 1.1) \times 10^2$
	$B(E2; 7_1^+ \to 5_1^+)$	4.37	1.4 ± 0.3
	$\mu(5_1^+)$	3.93	3.917 ± 0.008
	$\mu(2_1^+)$	4.88	$+3.7 \pm 0.2$
^{106}Ag	$\mu(1_1^+)$	3.03	$+2.9 \pm 0.2$
	$Q(6_1^+)$	0.73	$+1.08 \pm 0.06$
	$\mu(6_1^+)$	4.08	$(+)3.705 \pm 0.004$
^{108}Ag	$B(E2; 1_2^+ \to 1_1^+)$	30.61	>3.1
	$B(E2; 3_1^+ \to 1_1^+)$	7.33	0.85 ± 0.08
	$B(M1; 2_1^+ \to 1_1^+)$	0.02	>0.012
	$B(M1; 1_2^+ \to 1_1^+)$	0.00	>0.0056
	$\mu(1_1^+)$	3.00	2.6884 ± 0.0007
	$Q(6_1^+)$	0.89	$+1.32 \pm 0.07$
	$\mu(3_1^+)$	3.33	3.888 ± 0.015
	$\mu(6_1^+)$	3.93	3.58 ± 0.02
^{110}Ag	$Q(1_1^+)$	0.06	0.24 ± 0.12
	$\mu(1_1^+)$	3.05	2.7271 ± 0.0008
	$Q(6_1^+)$	-0.03	$+1.41 \pm 0.10$
	$\mu(6_1^+)$	4.19	$+3.607 \pm 0.004$
	$\mu(3_1^+)$	3.53	$+3.77 \pm 0.03$

IV. β-DECAY PROPERTIES

A. $\log_{10} ft$ values

The wave functions of the initial and final states resulting from the IBM-2 and IBFFM-2 Hamiltonians are used to calculate the matrix elements of the GT operator (15), denoted by $M^{\rm GT}$, which are necessary to obtain ft values in seconds:

$$ft = \frac{6163}{\left(\frac{g_{\rm A}}{g_{\rm V}}\right)^2 |M^{\rm GT}|^2}. \tag{23}$$

$g_{\rm A} = 1.27$ and $g_{\rm V} = 1$ are the free values of the axial vector and vector coupling constants, respectively. In order to better describe the β-decay rate, effective $g_{\rm A}$ factors are often considered by quenching the free value. As shown in the following, the effective $g_{\rm A}$ values that could be estimated from the observed $\log_{10} ft$ values are quite at variance with different nuclei; that is, in some cases the $g_{\rm A}$ factor would need to be reduced, while in other cases it should be increased. For the sake of simplicity, the free value, $g_{\rm A} = 1.27$, is used throughout in the present study for calculating ft values.

In Figs. 7(a)–7(f) the calculated $\log_{10} ft$ values for the β^- decay of the 0_1^+ ground state of even-even nuclei into the 1_1^+ state of the odd-odd nuclei are presented as functions of N for each isotopic chain. One notices that the $0_1^+ \to 1_1^+ \beta^-$-decay $\log_{10} ft$ values are systematically lower than the measured ones [73], mainly in those nuclei located before the shape phase transitions, i.e., $N \leqslant 60$, and with lower proton numbers, i.e., Kr, Sr, and Zr ones. This finding indicates that an enormous amount of quenching would need to be made of the GT transition matrix elements. In the case of the $^{98}{\rm Sr}(0_1^+) \to {}^{98}{\rm Y}(1_1^+)$ decay, for instance, an effective $g_{\rm A}$ factor that is one order of magnitude smaller than the free value $g_{\rm A} = 1.27$ would be required to reproduce the experimental $\log_{10} ft$ value of 4.9 ± 0.1 [73].

As often suggested (see, e.g., Ref. [25]), the quenching of the GT matrix elements implies certain deficiencies of the employed nuclear structure models regarding, e.g., various model assumptions, parameters, and restricted configuration spaces. In the present case, indeed, the assumption of taking only the $g_{9/2}$ orbital for the proton single-particle space seems reasonable for those isotopes with Z being near the $Z = 50$ major shell closure, for which the $g_{9/2}$ orbital plays an predominant role, whereas for the low-Z nuclei, which are rather close to the $Z = 28$ major shell closure, some other single-particle states, such as those coming from outside of the $Z = 28$–50 major shell, may play a role.

The calculated GT matrix element can be analyzed by decomposing it into components that are associated with different neutron-proton pair configurations. For the $^{98}{\rm Sr}(0_1^+) \to {}^{98}{\rm Y}(1_1^+)$ decay, for example, the dominant contribution to the GT transition comes from the matrix elements of the terms in the GT operator that are of the forms like $[a^\dagger_{\nu g_{7/2}} \times a^\dagger_{\pi g_{9/2}}]^{(1)}$ and $[\tilde{d}_\nu \times [a^\dagger_{\nu g_{7/2}} \times a^\dagger_{\pi g_{9/2}}]^{(L)}]^{(1)}$, which are calculated to be too large in magnitude, thus leading to the small $\log_{10} ft$ values.

One can also observe in Figs. 7(a)–7(f) that for the β^- decays of the Zr and Mo isotopes the calculated $\log_{10} ft$ values exhibit a drastic increase around $N = 60$. In the Mo isotopic chain, the predicted $\log_{10} ft$ values are even larger than the measured ones for the heavier isotopes with $N \geqslant 62$. Here, the rapid increase of the $\log_{10} ft$ values at $N \approx 60$ could be also explained by the dominance of the neutron-proton pair configuration in the IBFFM-2 1_1^+ wave functions. As mentioned above, for those nuclei with $N \leqslant 60$, the matrix elements of the terms that involve the pair configurations of the type $[\nu g_{7/2} \otimes \pi g_{9/2}]^{(J)}$ are shown to be large. However, this does not seem to be the case for the nuclei with $N > 60$, where in the corresponding 1_1^+ wave functions some other pair configurations start to make appreciable contributions (see, Fig. 6). The different pair components are more or less fragmented in the GT matrix elements for the $N > 60$ nuclei, and cancel each other to give rise to the rather small $M^{\rm GT}$, or large $\log_{10} ft$ value.

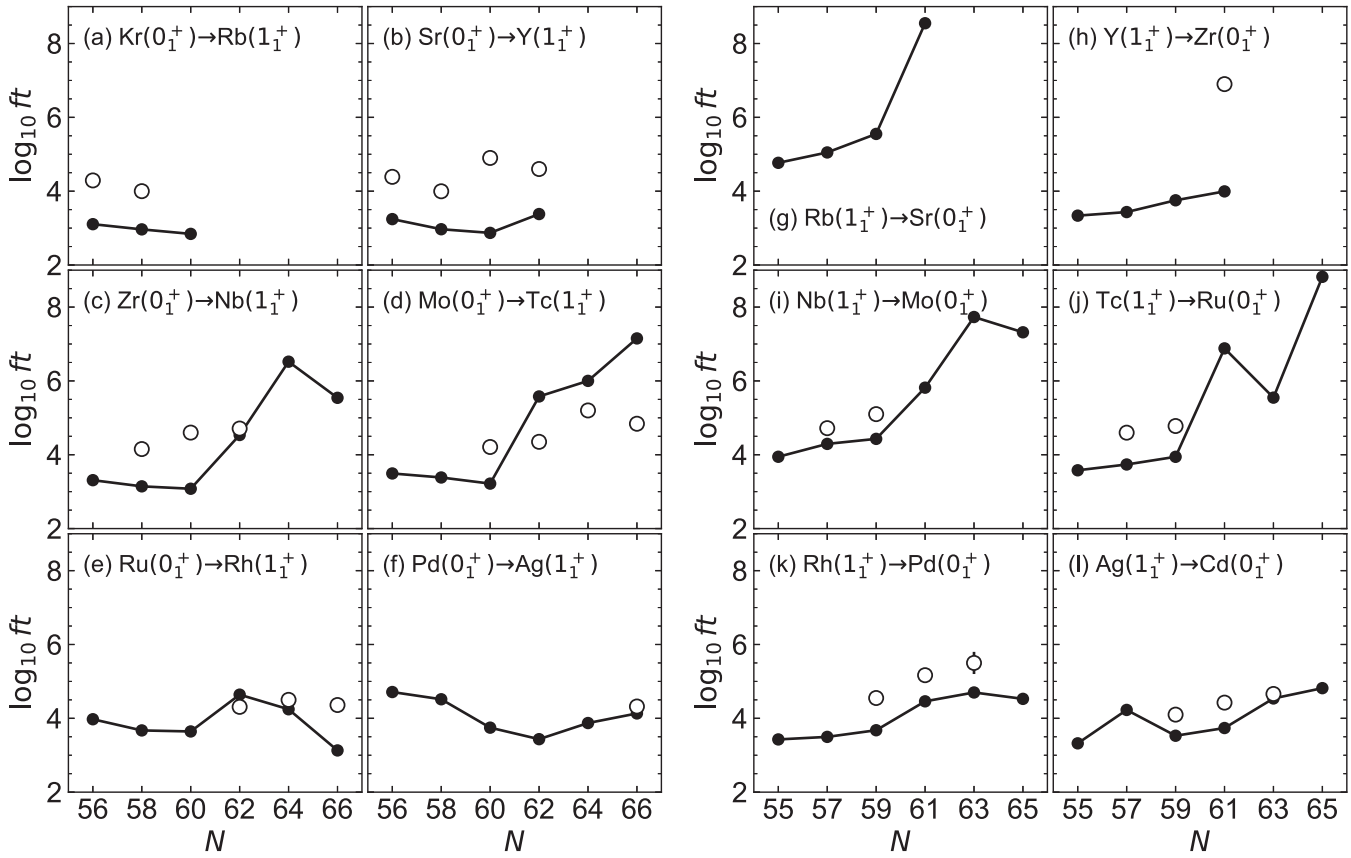

FIG. 7. The $\log_{10} ft$ values for [(a)–(f)] the β^- decay of the 0_1^+ ground state of even-even nuclei into the 1_1^+ state of odd-odd nuclei, and [(g)–(l)] the β^- decay of the 1_1^+ state of odd-odd nuclei into the 0_1^+ state of even-even nuclei. Calculated $\log_{10} ft$ values are represented by solid circles connected by lines, and open circles denote the experimental values [73].

Given that the $\log_{10} ft$ values increase sharply for the $N > 60$ even-even nuclei, and that in some cases [e.g., the Mo decays in Fig. 7(d)] overestimate the data, then the g_A factor would need to be rather increased for these neutron-rich isotopes, whereas a quenched g_A factor would be required for the lighter isotopes with $N \leqslant 60$. As mentioned earlier, an immediate cause of this peculiarity is the change with N in the nature of the wave functions for the odd-odd nuclei. The nuclear wave functions should be, however, sensitive to the choice of the single-particle spaces, Hamiltonian parameters, and single-particle properties ($\tilde{\epsilon}_{j_\rho}$ and $v^2_{j_\rho}$), which are determined largely by the underlying EDF-SCMF calculation, and are at variance with different EDFs. This point is pursued further in Sec. IV C. The sensitivity of the mapped IBM-2 prediction of the $2\nu\beta\beta$-decay NMEs to the single-particle spaces and to the different EDFs has also been addressed in Ref. [56].

As compared to the $0_1^+ \to 1_1^+$ β^- decay of the lighter even-even nuclei with $N \leqslant 60$ and $Z < 40$, variation of the $\log_{10} ft$ values with N occurs much more slowly for the Ru(0_1^+) → Rh(1_1^+) [Fig. 7(e)] and Pd(0_1^+) → Ag(1_1^+) [Fig. 7(f)] β^- decays.

In a similar fashion, in Figs. 7(g)–7(l) the predicted $\log_{10} ft$ values for the β^- decay of the odd-odd nuclei are compared with the experimental counterparts [73]. Experimental data are not available for the Rb(1_1^+) → Sr(0_1^+) decay, and only the lower bound, $\log_{10} ft > 6.9$, of the unidentified $(1)^-$ state is known for the ^{100}Y(1_1^+) → ^{100}Zr(0_1^+) decay. A general remark is that in each isotopic chain the calculated $1_1^+ \to 0_1^+$ $\log_{10} ft$ value increases as a function of N, consistently with the observed systematic, and further exhibits a rapid increase from $N = 59$ to 61. The change is particularly significant for the Nb(1_1^+) → Mo(0_1^+) and Tc(1_1^+) → Ru(0_1^+) decays, while for the Rh(1_1^+) → Pd(0_1^+) and Ag(1_1^+) → Cd(0_1^+) ones the predicted $\log_{10} ft$ values increase more slowly with N. In addition, the present calculation reproduces the measured $\log_{10} ft$ values to a greater extent than in the case of the β^- decay of the even-even nuclei.

In addition to the transitions between the 0_1^+ and 1_1^+ states, there are $\log_{10} ft$ data for the decays between states with spin other than 1^+ and between higher-lying 0^+ and 1^+ states. To keep the discussion as simple as possible, let us focus on the β decays that only involve the even-even $N = 60$ isotones. The calculated and experimental [73] $\log_{10} ft$ values of the β^- and EC decays are listed in Tables IV and V, respectively. As one can see from Table IV, it is rather hard to draw a solid conclusion on the quality of the mapped IBM-2 framework for the description of the $\log_{10} ft$ values for many different β^- decays. Nevertheless, for many of the low-Z nuclei, the present

TABLE IV. Comparison of calculated and observed [73] $\log_{10} ft$ values for the β^- decay of the even-mass nuclei including the $N = 60$ isotones.

Decay	$I \to I'$	$\log_{10} ft$ Theor.	$\log_{10} ft$ Expt.
^{98}Rb $\to$ ^{98}Sr	$3_1^+ \to 2_1^+$	7.78	5.6
	$3_1^+ \to 2_2^+$	9.95	6.2
	$3_1^+ \to 2_3^+$	8.44	6.1
	$3_1^+ \to 2_4^+$	8.05	5.5
	$3_1^+ \to 4_1^+$	7.90	6.3
^{98}Sr $\to$ ^{98}Y	$0_1^+ \to 1_1^+$	2.87	4.9 ± 0.1
	$0_1^+ \to 1_2^+$	4.38	4.4 ± 0.1
	$0_1^+ \to 1_3^+$	4.82	5.5 ± 0.1
	$0_1^+ \to 1_4^+$	4.20	5.6 ± 0.1
^{100}Y $\to$ ^{100}Zr	$4_1^+ \to 3_1^+$	4.22	>6.5
	$4_1^+ \to 4_1^+$	5.46	≈6.0
	$4_1^+ \to 4_2^+$	4.54	>6.6
	$4_1^+ \to 4_3^+$	4.83	>6.9
^{100}Zr $\to$ ^{100}Nb	$0_1^+ \to 1_1^+$	3.08	4.6 ± 0.1
	$0_1^+ \to 1_2^+$	3.90	4.8 ± 0.1
	$0_1^+ \to 1_3^+$	6.50	5.8
	$0_1^+ \to 1_4^+$	6.34	4.5 ± 0.1
^{102}Nb $\to$ ^{102}Mo	$1_1^+ \to 0_1^+$	5.82	
	$1_1^+ \to 0_2^+$	6.99	
	$1_1^+ \to 2_1^+$	6.72	
	$1_1^+ \to 2_2^+$	7.53	
	$4_1^+ \to 3_1^+$	6.45	6.21
	$4_1^+ \to 3_2^+$	6.20	4.86
	$4_1^+ \to 4_1^+$	7.51	6.44
	$4_1^+ \to 4_2^+$	7.45	6.31
^{102}Mo $\to$ ^{102}Tc	$0_1^+ \to 1_1^+$	3.22	4.21 ± 0.09
	$0_1^+ \to 1_2^+$	4.48	5.74 ± 0.10
	$0_1^+ \to 1_3^+$	5.19	4.81 ± 0.09
^{104}Tc $\to$ ^{104}Ru	$3_1^+ \to 2_1^+$	6.22	8.10 ± 0.07
	$3_1^+ \to 2_2^+$	5.63	8.14 ± 0.09
	$3_1^+ \to 3_1^+$	7.83	8.18 ± 0.10
	$3_1^+ \to 4_1^+$	6.91	8.34 ± 0.09
^{106}Rh $\to$ ^{106}Pd	$1_1^+ \to 0_1^+$	4.46	5.168 ± 0.007
	$1_1^+ \to 0_2^+$	6.45	5.354 ± 0.019
	$1_1^+ \to 0_3^+$	7.15	5.51 ± 0.05
	$1_1^+ \to 0_4^+$	7.62	5.63 ± 0.07
	$1_1^+ \to 2_1^+$	4.11	5.865 ± 0.017
	$1_1^+ \to 2_2^+$	7.72	6.55 ± 0.07
	$1_1^+ \to 2_3^+$	6.48	5.757 ± 0.017
	$1_1^+ \to 2_4^+$	6.35	6.25 ± 0.03
	$1_1^+ \to 2_5^+$	5.06	5.83 ± 0.03
	$1_1^+ \to 2_6^+$	7.52	6.59 ± 0.10
^{108}Ag $\to$ ^{108}Cd	$1_1^+ \to 0_1^+$	3.74	4.425 ± 0.009
	$1_1^+ \to 2_1^+$	6.06	5.35 ± 0.03

calculation gives smaller $\log_{10} ft$ values than the experimental ones, suggesting that the assumption of considering only the single proton orbital ($\pi g_{9/2}$) may not be reasonable, and that the $\log_{10} ft$ calculations are also influenced by the chosen parameters or forms of the IBFFM-2 Hamiltonian. The calculation, however, overestimates the measured $\log_{10} ft$ values for higher-Z nuclei.

TABLE V. Same as Table IV, but for the EC decay.

Decay	$I \to I'$	$\log_{10} ft$ Theor.	$\log_{10} ft$ Expt.
^{104}Rh $\to$ ^{104}Ru	$1_1^+ \to 0_1^+$	4.12	4.32 ± 0.11
	$1_1^+ \to 0_2^+$	4.93	5.15 ± 0.18
	$1_1^+ \to 2_1^+$	6.26	5.42 ± 0.06
^{106}Ag $\to$ ^{106}Pd	$1_1^+ \to 0_1^+$	4.22	4.92
	$1_1^+ \to 0_2^+$	4.48	6.5
	$1_1^+ \to 0_3^+$	5.32	7.0
	$1_1^+ \to 0_4^+$	5.88	6.1
	$1_1^+ \to 0_5^+$	6.65	7.6
	$1_1^+ \to 0_6^+$	5.89	7.2
	$1_1^+ \to 0_7^+$	5.25	6.6
	$1_1^+ \to 2_1^+$	5.02	5.24
	$1_1^+ \to 2_2^+$	5.74	6.5
	$1_1^+ \to 2_3^+$	5.02	7.9
	$1_1^+ \to 2_4^+$	5.93	6.9
	$1_1^+ \to 2_5^+$	4.40	6.8
	$1_1^+ \to 2_6^+$	5.41	7.8
	$6_1^+ \to 6_1^+$	8.95	8.02 ± 0.24
	$6_1^+ \to 5_1^+$	7.74	5.087 ± 0.018
	$6_1^+ \to 5_2^+$	7.57	5.08 ± 0.5

Experimental data for the $\log_{10} ft$ values for the EC decay are available for the ^{104}Rh and ^{106}Ag nuclei. Overall, the present calculation reproduces the $\log_{10} ft$ data fairly well, especially for those nuclei that are not very far from the proton $Z = 50$ major shell.

B. GT strength distributions

On the left-hand side of Fig. 8, distributions of the B(GT) transition strengths, $B(\mathrm{GT}; 0_1^+ \to 1_1^+) = |M^{\mathrm{GT}}(0_1^+ \to 1_1^+)|^2$, for the β^- decay of the even-even $N = 60$ isotones are shown as functions of the 1^+ excitation energies $E(1_n^+)$ below 8 MeV. For the decays of ^{98}Sr, ^{100}Zr, and ^{102}Mo, experimental B(GT) values are shown, which are obtained by using the corresponding $\log_{10} ft$ data and the formula in Eq. (23). Error bars for the experimental B(GT) values are not shown, since they are smaller than the size of the symbols in the plot.

For each odd-odd nucleus, all the 1^+ states resulting from the IBFFM-2 and the corresponding GT transitions are here considered. For most of the even-even nuclei shown in the figure, the GT transition to the first excited 1_1^+ is the strongest, while contributions from the decays to higher-lying 1^+ states become more minor with the increasing 1^+ excitation energy. For the ^{104}Ru$(0_1^+) \to$ ^{104}Rh(1^+) decay, in particular, non-negligible amounts of the GT transitions are predicted within the excitation energies $E(1_n^+)$ from around 2 to 4 MeV. A similar degree of the fragmentation of the B(GT) strength distributions are obtained for the ^{102}Mo$(0_1^+) \to$ ^{102}Tc(1^+) decay below $E(1_n^+) \approx 2$ MeV. The predicted GT strengths for the ^{98}Sr, ^{100}Zr, and ^{102}Mo nuclei are, in some cases, larger by about an order of magnitude, but agree rather well with the observed systematic that the GT transitions to the low-lying 1^+ states are dominant.

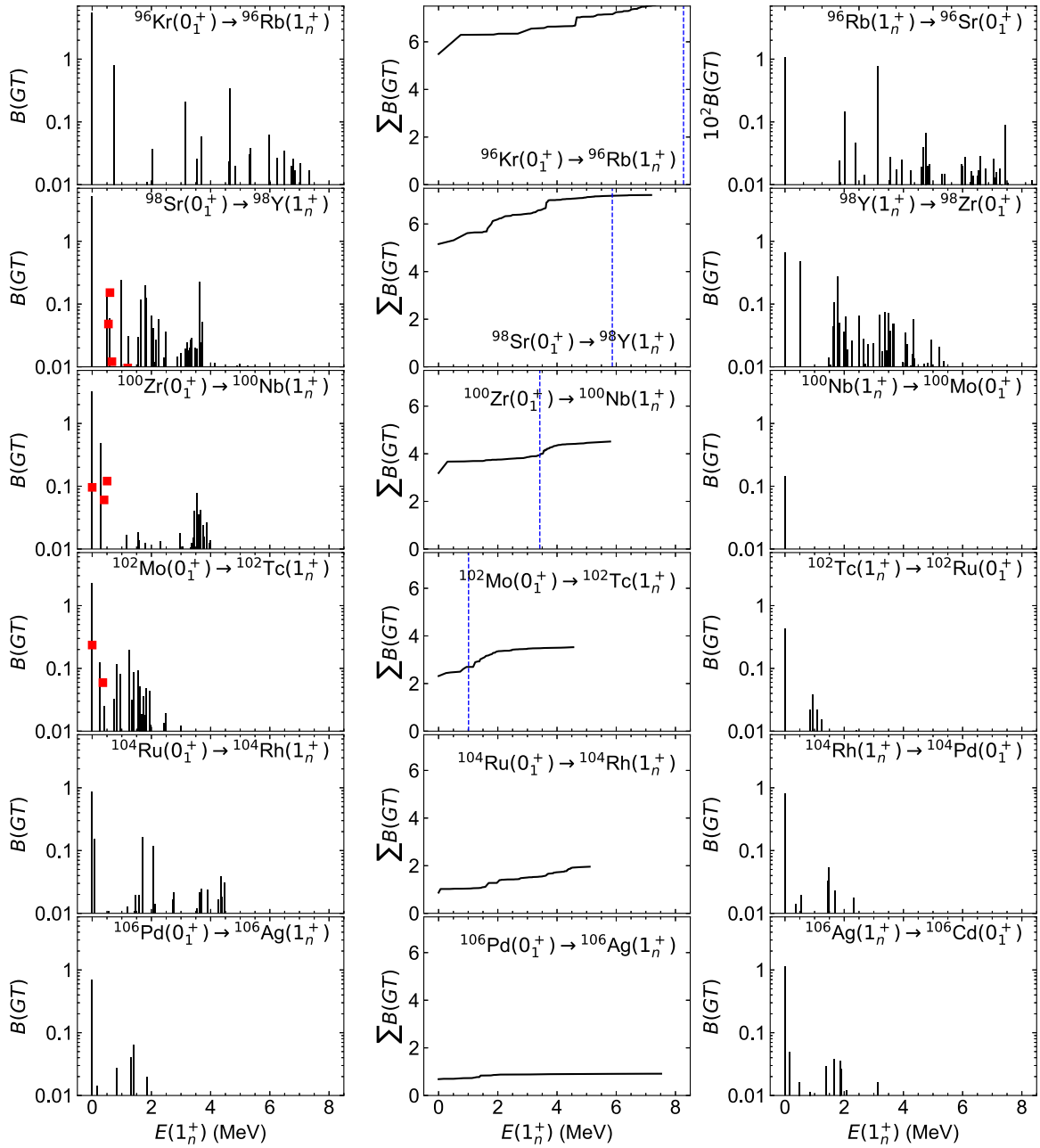

FIG. 8. B(GT) strength distribution for the β^- decay $0_1^+ \to 1_n^+$ of the even-even $N = 60$ isotones in terms of the excitation energies of the 1_n^+ states of the odd-odd final nuclei (left), their running sum (middle), and B(GT) strength distribution for the β^- decay $1_n^+ \to 0_1^+$ of the odd-odd $N = 59$ isotones (right). The experimental $B(\mathrm{GT}; 0_1^+ \to 1^+)$ values extracted from the $\log_{10} ft$ data [73] are shown as red squares. The dashed vertical lines in the middle panels indicate experimental Q_{β^-} values [73]. Note that the B(GT) values for the ^{96}Rb(1_n^+) → ^{96}Sr(0_1^+) are too small, and they are scaled with a factor of 100 so that they are more visible.

In addition, in the middle column of Fig. 8, running sums of the GT strengths, i.e., $\sum_n B(\mathrm{GT}; 0_1^+ \to 1_n^+)$, that are taken up to the excitation energy of the highest-lying 1^+ state are shown. Experimental Q_{β^-} values for the ^{96}Kr, ^{98}Sr, ^{100}Zr, and ^{102}Mo are also indicated in the figure. Note that, as ^{104}Ru and ^{106}Pd are stable nuclei, the corresponding Q_{β^-} values are negative and thus not shown in the figure. For most of the considered β^- decays, the sums appear to converge at low excitation energy, typically of $E(1^+) \leqslant 4$ MeV. Especially for the ^{98}Sr(0_1^+) → ^{98}Y(1^+) and ^{100}Zr(0_1^+) → ^{100}Nb(1^+) decays, the running sum more or less becomes constant before and around the measured Q_{β^-} values, respectively. Notably for the ^{96}Kr(0_1^+) → ^{96}Rb(1^+) and ^{104}Ru(0_1^+) → ^{104}Rh(1^+) decays, the sums continue to increase up to the excitation energies of the highest-lying 1^+ states obtained with the IBFFM-2. The GT decay rates are predicted to be remarkably large for the low-Z isotones, i.e., ^{96}Kr and ^{98}Sr, with the corresponding running sums reaching $\sum_n B(\mathrm{GT}; 0_1^+ \to 1_n^+) \approx 7.5$.

For higher-Z, stable nuclei, e.g., ^{106}Pd, the final sum becomes smaller, $\sum_n B(\mathrm{GT}; 0_1^+ \to 1_n^+) < 1$. This conforms to the results shown in Fig. 7, that the calculated $\log_{10} ft$ values for the GT transition of the even-even nuclei to the lowest 1^+ state of the odd-odd nuclei are particularly small for the low-Z nuclei such as Kr and Sr ones.

On the right-hand side of Fig. 8, the B(GT) strength distributions, $B(\mathrm{GT} : 1_1^+ \to 0_1^+) = |M^{\mathrm{GT}}(1_1^+ \to 0_1^+)|^2/3$, for the β^- decays of the odd-odd $N = 59$ into the even-even $N = 58$ isotones are depicted in terms of the $E(1^+)$ excitation energy. In general, the GT strengths for the odd-odd isotones are predicted to be smaller, <1.0, than those for the even-even nuclei, which are larger than 1 (see left column of Fig. 8). As in the case of the even-even nuclei, contributions from the low-lying 1^+ states are dominant also for the β^- decays of odd-odd nuclei, such as ^{100}Nb, ^{102}Tc, ^{104}Rh, and ^{106}Ag. Of particular interest are the $^{96}\mathrm{Rb}(1^+) \to {}^{96}\mathrm{Sr}(0_1^+)$ and $^{98}\mathrm{Y}(1^+) \to {}^{98}\mathrm{Zr}(0_1^+)$ decays. For these decay processes, the B(GT) strength distribution exhibits a substantial degree of fragmentation, and contributions from the nonyrast 1^+ states are as significant as that from the lowest 1^+ state. Note that, as for the B(GT) rate of the $^{96}\mathrm{Rb}(1^+) \to {}^{96}\mathrm{Sr}(0_1^+)$ decay, the B(GT) rates are negligibly small, so that they are scaled with a factor of 100 in the figure.

Summarizing the results shown in Fig. 8, it appears that the GT transitions of the lowest- or low-lying 1^+ states make dominant roles in the running sums of the B(GT) strengths for the β^- decays of both the even-even and odd-odd nuclei, while the fragmentation tends to occur for those nuclei far from the proton $Z = 50$ major shell closure. This observation seems compatible, to a good extent, to the single-state dominance [76,77] or the low-lying state dominance [78] proposed especially for the studies of double-β decay. The previous mapped IBM-2 calculation in Ref. [56] has also provided a similar conclusion on the $2\nu\beta\beta$ decay NMEs of a number of candidate nuclei. The finding in the present calculation, that the GT transition strength is dominated by the low-lying 1^+ states, sheds light upon the interpretation of the dominance in the GT strength, as it varies significantly with both the measurements and different theoretical approaches.

It should be also worth investigating how the GT strength distribution changes along a given isotopic chain, particularly toward the neutron-rich region that is experimentally of much relevance. For that purpose, the B(GT) strength distributions and their running sums for β^- decays of the even-even Zr isotopes are shown in Fig. 9. For ^{96}Zr, ^{98}Zr, and ^{100}Zr, the GT strength is almost solely accounted for by the transition to the first 1^+ state, which is also considerably large in magnitude, $B(\mathrm{GT}; 0_1^+ \to 1_1^+) \approx 2$–3. However, one notices for the heavier Zr nuclei, i.e., ^{102}Zr, ^{104}Zr, and ^{106}Zr, that the GT strength is fragmented to a great extent. Particularly for the $^{104}\mathrm{Zr}(0_1^+) \to {}^{104}\mathrm{Nb}(1^+)$ decay, the major contribution to the total GT strength comes from the transitions to the 1^+ states that are at the excitation energy $E(1^+)$ of about 4–6 MeV, while the $B(\mathrm{GT}; 0_1^+ \to 1_1^+)$ transition does not play a significant role. For the lighter Zr nuclei, e.g., ^{96}Zr and ^{98}Zr, the sum, $\sum_n B(\mathrm{GT})$, appears to be converged at relatively low $E(1^+)$ excitation energies, $E(1^+) \approx 2$ MeV, and the convergence is reached near the measured Q_{β^-} values. Note that ^{96}Zr is a candidate nucleus for the $0\nu\beta\beta$ decay. However, for the heavier Zr isotopes, ^{102}Zr, ^{104}Zr, and ^{106}Zr, the convergence seems to occur at higher $E(1^+)$ excitation energies, e.g., $E(1^+) > 4$ MeV, that are larger or in the vicinity of the Q_{β^-} values.

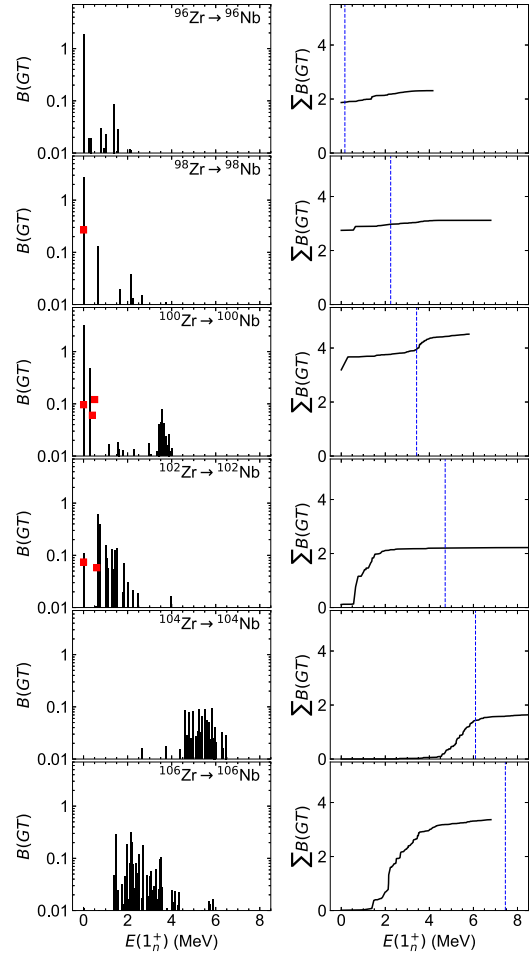

FIG. 9. B(GT) strength distribution for the β^- decay $0_1^+ \to 1_n^+$ of the Zr isotopes in terms of the excitation energies $E(1_n^+)$ of the final Nb nuclei (left), and their running sums (right).

C. Sensitivity to the choice of EDF

As a possible source of the theoretical uncertainty, in this section sensitivity of the $\log_{10} ft$ predictions to the choice of the EDF is explored. The $^{106}\mathrm{Rh} \to {}^{106}\mathrm{Pd}$ decay is considered as an illustration, since this decay was also studied within the mapped IBM-2/IBFFM-2 framework in Ref. [55], where the D1M interaction [79] of the Gogny EDF was employed as the microscopic input for the IBM-2 and IBFFM-2. The present calculation with the DD-PC1 EDF generally gives larger $\log_{10} ft$ values than that based on the Gogny-D1M EDF. For example, the Gogny-D1M EDF calculation of Ref. [55] provided the $\log_{10} ft$ value of the $1_1^+ \to 0_1^+$ decay to be 3.31, while the present value is 4.46 (see Table IV), which is larger than the former by an order of magnitude in ft values.

TABLE VI. Strength parameters for the IBFFM-2 Hamiltonian for the ^{106}Rh nucleus employed in the present work (DD-PC1) and in the previous calculation that is based on the Gogny-D1M EDF [79], reported in Ref. [55]. All the parameters, but for χ_ν and χ_π, are in MeV units.

EDF	ϵ	κ	χ_ν	χ_π	κ'	Γ_ν	Λ_ν	A_ν	Γ_π	Λ_π	A_π	$v_{\rm d}$	$v_{\rm t}$
DD-PC1	0.18	−0.364	−0.5	−0.38	0.032	0.3	0	0	0.3	1.2	0	−0.08	0.05
D1M	0.85	−0.301	−0.86	−0.6	0	0.7	0.7	0	0.6	0.6	0	−0.20	0.1

Table VI compares the IBFFM-2 parameters for ^{106}Rh obtained with the DD-PC1 and Gogny-D1M EDFs. Differences in the parameters for the IBM-2 Hamiltonian are due to the different nature of the PESs provided by the two functionals. In both cases, the (β, γ) PES for the even-even core nucleus, ^{106}Pd, shows a weak prolate deformation typically at $\beta \approx 0.2$ (see Fig. 1, and Fig. 2 of Ref. [55]). The DD-PC1 PES, however, exhibits a steeper potential valley than the D1M counterpart. This is reflected in the differences in the derived parameters, e.g., ϵ and κ, shown in Table VI. Furthermore, in Table VII the quasiparticle energies, $\tilde{\epsilon}_{j_\rho}$, and occupation probabilities, $v^2_{j_\rho}$, for the odd neutron and odd proton, which are used in determining the IBFFM-2 interaction strength and β-decay operators, are compared between the mapped IBM-2 calculations based on the DD-PC1 and Gogny-D1M EDFs. These single-particle properties are crucial to determine the boson-fermion and fermion-fermion interactions, but are at variance with the EDFs.

Figure 10 compares the energy spectra for the ^{106}Pd and ^{106}Rh nuclei between the calculations based on the DD-PC1 and Gogny-D1M EDFs. In general, the mapped IBM-2 calculation with the DD-PC1 EDF gives a better description of the energy spectra for ^{106}Pd than that employing the D1M EDF. The D1M-IBM-2 energy spectrum exhibits a rotational feature and is rather stretched in energy with increasing angular momentum, as compared to the DD-PC1 result. The difference arises mainly from the parameters χ_ν and χ_π, which are responsible for the γ softness. Especially when the absolute value of the average, $\chi = |\chi_\nu + \chi_\pi|/2$, is chosen to be large, then it generally leads to a rotational-like level structure. One actually sees from Table VI that both the parameters χ_ν and χ_π employed in the previous IBM-2 study [55] with the D1M EDF are larger in magnitude than those in the present calculation using the DD-PC1 EDF.

Similarly, for the odd-odd nucleus, ^{106}Rh, the energy spectra obtained from the two EDFs are rather different, that is, the calculation employing the DD-PC1 EDF reproduces better the 6^+_1 energy level, while in the D1M energy spectrum the 2^+_1 and 5^+_1 levels come below the 6^+_1 level. In addition, the IBFFM-2 calculation with the DD-PC1 EDF gives nonyrast 1^+ energy levels that are lower than in the case of the D1M EDF. In the DD-PC1 EDF calculation, the structure of the IBFFM-2 1^+_1 state for ^{106}Rh is described by the neutron-proton pair configurations $[\nu g_{7/2} \otimes \pi g_{9/2}]^{(J=1)}$ and $[\nu g_{7/2} \otimes \pi g_{9/2}]^{(J=3)}$, which share, respectively, 52% and 43% of the wave function. In the IBFFM-2 calculation of Ref. [55] using the Gogny-D1M EDF, however, only the $[\nu g_{7/2} \otimes \pi g_{9/2}]^{(J=1)}$ pair component plays a predominant role (73%) to determine the 1^+_1 wave function, whereas there are numerous minor contributions from other pair configurations. This difference more or less explains the discrepancies in the $\log_{10} ft$ values between the two EDFs, since in the Gogny-D1M case matrix elements of the terms in the GT operator that contain the pair $[\nu g_{7/2} \otimes \pi g_{9/2}]^{(J=1)}$ are quite large, but those of other terms cancel each other to a greater extent than in the case of the DD-PC1 EDF.

TABLE VII. The quasiparticle energies, $\tilde{\epsilon}_{j_\rho}$ (in MeV), and occupation probabilities, $v^2_{j_\rho}$, for the single-particle orbitals used in the mapped IBM-2 calculations employing the DD-PC1 and D1M EDFs.

EDF		$\nu 3s_{1/2}$	$\nu 2d_{3/2}$	$\nu 2d_{5/2}$	$\nu 1g_{7/2}$	$\pi 1g_{9/2}$
DD-PC1	$\tilde{\epsilon}_{j_\rho}$	1.883	2.148	1.674	1.760	1.463
	$v^2_{j_\rho}$	0.158	0.147	0.705	0.693	0.522
D1M	$\tilde{\epsilon}_{j_\rho}$	3.706	4.446	1.863	3.214	1.166
	$v^2_{j_\rho}$	0.333	0.179	0.843	0.496	0.516

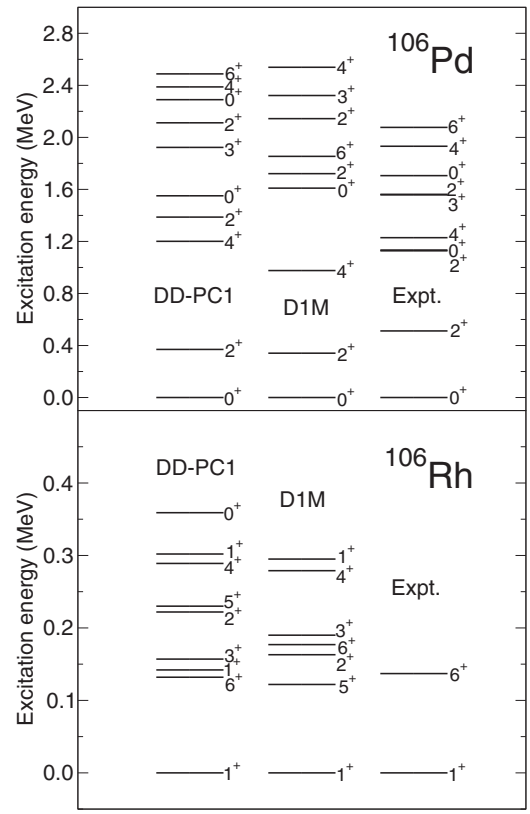

FIG. 10. Low-energy spectra for the ^{106}Pd and ^{106}Rh nuclei computed with the microscopic inputs provided from the DD-PC1 and Gogny-D1M EDFs. The experimental data are taken from Ref. [73], and the results for the Gogny-D1M EDF are exploited from Ref. [55].

As it is also evident from the comparisons in Tables VI, VII and Fig. 10, the parameters for the IBFFM-2 and single-particle properties depend largely on the choice of the EDF, which then lead to the differences in the predicted excitation spectra and $\log_{10} ft$ values. It remains, however, an open issue to identify which parameters are most responsible for the different $\log_{10} ft$ value predictions in the employed theoretical approach.

V. SUMMARY AND CONCLUSIONS

The low-energy structure and β-decay properties of the neutron-rich even-mass nuclei around $N = 60$ that are currently under extensive investigations have been studied within the theoretical framework of the EDF-to-IBM mapping. The IBM-2 Hamiltonian describing the even-even core nuclei, and particle-boson interactions, have been determined by using the results of the triaxial quadrupole constrained SCMF calculations within the RHB model with the DD-PC1 functional and the separable pairing force. The resulting wave functions for the initial and final nuclei, obtained from the IBM-2 and IBFFM-2, have been used to compute the GT transition strengths, where the corresponding operators have been constructed without introducing adjustable parameters.

The calculated (β, γ) PESs for the $N = 60$ even-even isotones suggest for most cases notably γ-soft shapes that vary substantially with Z. Spectroscopic calculations for the even-even Kr, Sr, Zr, Mo, Ru, Pd, and Cd isotopes within the mapped IBM-2 have produced evolution of the low-lying energy spectra and $B(E2)$ rates as functions of N, and rapid changes of these observables around $N = 60$ along the Sr, Zr, and Mo isotopic chains. The excitation spectra of low-spin states of the neighboring odd-odd nuclei have been shown to exhibit certain variation with N, reflecting the shape transitions that occur in the even-even core nuclei.

The mapped IBM-2 and IBFFM-2 calculation has provided the $\log_{10} ft$ values for the β^- decays of the 0_1^+ state of the even-even nuclei into the 1_1^+ state of the odd-odd nuclei that are systematically lower than the experimental values for the lower-Z isotopes (i.e., Kr, Sr, and Zr) and mostly for $N \leqslant 60$. The too small $\log_{10} ft$ values in these nuclear systems indicate a need for a substantial degree of quenching for the $g_{\rm A}$ factor, which amounts to an order of magnitude in some cases. For those nuclei with $N > 60$ and higher Z, however, the calculated $\log_{10} ft$ values exhibit a sharp increase with N, and especially for Mo isotopes the calculation overestimates the data. The necessity of introducing effective $g_{\rm A}$ factors would then imply deficiencies of the theoretical framework that arise from various model assumptions and approximations, including the particular choice of the EDF providing microscopic input to the IBM-2 and IBFFM-2, the form of the corresponding Hamiltonians, and the restricted single-particle space. The sensitivity of the results to the choice of the nuclear EDF has been explored, specifically, by comparing the calculations that employ the relativistic DD-PC1 and nonrelativistic Gogny-D1M EDFs as the microscopic inputs to the IBM-2 and IBFFM-2.

The simultaneous calculation of the low-energy nuclear structure and β decay will be useful for improving the quality of the employed theoretical method in describing spectroscopic properties of individual nuclei even more accurately, and will provide implications for studies of other fundamental nuclear processes including the $0\nu\beta\beta$ decay.

[1] P. Cejnar, J. Jolie, and R. F. Casten, Rev. Mod. Phys. **82**, 2155 (2010).
[2] K. Heyde and J. L. Wood, Rev. Mod. Phys. **83**, 1467 (2011).
[3] E. Caurier, G. Martínez-Pinedo, F. Nowacki, A. Poves, and A. P. Zuker, Rev. Mod. Phys. **77**, 427 (2005).
[4] K. Sieja, F. Nowacki, K. Langanke, and G. Martínez-Pinedo, Phys. Rev. C **79**, 064310 (2009).
[5] T. Togashi, Y. Tsunoda, T. Otsuka, and N. Shimizu, Phys. Rev. Lett. **117**, 172502 (2016).
[6] N. Shimizu, T. Abe, M. Honma, T. Otsuka, T. Togashi, Y. Tsunoda, Y. Utsuno, and T. Yoshida, Phys. Scr. **92**, 063001 (2017).
[7] M. Bender, P.-H. Heenen, and P.-G. Reinhard, Rev. Mod. Phys. **75**, 121 (2003).
[8] D. Vretenar, A. V. Afanasjev, G. A. Lalazissis, and P. Ring, Phys. Rep. **409**, 101 (2005).
[9] T. Nikšić, D. Vretenar, and P. Ring, Prog. Part. Nucl. Phys. **66**, 519 (2011).
[10] H. Mei, J. Xiang, J. M. Yao, Z. P. Li, and J. Meng, Phys. Rev. C **85**, 034321 (2012).
[11] L. M. Robledo, T. R. Rodríguez, and R. R. Rodríguez-Guzmán, J. Phys. G: Nucl. Part. Phys. **46**, 013001 (2019).
[12] F. Iachello and A. Arima, *The Interacting Boson Model* (Cambridge University Press, Cambridge, UK, 1987).
[13] K. Nomura, R. Rodríguez-Guzmán, and L. M. Robledo, Phys. Rev. C **94**, 044314 (2016).
[14] J. E. García-Ramos and K. Heyde, Phys. Rev. C **102**, 054333 (2020).
[15] K. Nomura, T. Nikšić, and D. Vretenar, Phys. Rev. C **102**, 034315 (2020).
[16] N. Gavrielov, A. Leviatan, and F. Iachello, Phys. Rev. C **105**, 014305 (2022).
[17] I. Dillmann, K.-L. Kratz, A. Wöhr, O. Arndt, B. A. Brown, P. Hoff, M. Hjorth-Jensen, U. Köster, A. N. Ostrowski, B. Pfeiffer, D. Seweryniak, J. Shergur, and W. B. Walters (ISOLDE Collaboration), Phys. Rev. Lett. **91**, 162503 (2003).
[18] S. Nishimura, Z. Li, H. Watanabe, K. Yoshinaga, T. Sumikama, T. Tachibana, K. Yamaguchi, M. Kurata-Nishimura, G. Lorusso, Y. Miyashita, A. Odahara, H. Baba, J. S. Berryman, N. Blasi, A. Bracco, F. Camera, J. Chiba, P. Doornenbal, S. Go, T. Hashimoto *et al.*, Phys. Rev. Lett. **106**, 052502 (2011).
[19] M. Quinn, A. Aprahamian, J. Pereira, R. Surman, O. Arndt, T. Baumann, A. Becerril, T. Elliot, A. Estrade, D. Galaviz, T. Ginter, M. Hausmann, S. Hennrich, R. Kessler, K.-L. Kratz, G. Lorusso, P. F. Mantica, M. Matos, F. Montes, B. Pfeiffer *et al.*, Phys. Rev. C **85**, 035807 (2012).
[20] G. Lorusso, S. Nishimura, Z. Y. Xu, A. Jungclaus, Y. Shimizu, G. S. Simpson, P.-A. Söderström, H. Watanabe, F. Browne,

P. Doornenbal, G. Gey, H. S. Jung, B. Meyer, T. Sumikama, J. Taprogge, Z. Vajta, J. Wu, H. Baba, G. Benzoni, K. Y. Chae *et al.*, Phys. Rev. Lett. **114**, 192501 (2015).
[21] R. Caballero-Folch, C. Domingo-Pardo, J. Agramunt, A. Algora, F. Ameil, A. Arcones, Y. Ayyad, J. Benlliure, I. N. Borzov, M. Bowry, F. Calviño, D. Cano-Ott, G. Cortés, T. Davinson, I. Dillmann, A. Estrade, A. Evdokimov, T. Faestermann, F. Farinon, D. Galaviz *et al.*, Phys. Rev. Lett. **117**, 012501 (2016).
[22] P. Navrátil and J. Dobeš, Phys. Rev. C **37**, 2126 (1988).
[23] F. Dellagiacoma and F. Iachello, Phys. Lett. B **218**, 399 (1989).
[24] S. Brant, N. Yoshida, and L. Zuffi, Phys. Rev. C **70**, 054301 (2004).
[25] N. Yoshida and F. Iachello, Prog. Theor. Exp. Phys. **2013**, 043D01 (2013).
[26] E. Mardones, J. Barea, C. E. Alonso, and J. M. Arias, Phys. Rev. C **93**, 034332 (2016).
[27] K. Nomura, R. Rodríguez-Guzmán, and L. M. Robledo, Phys. Rev. C **101**, 024311 (2020).
[28] K. Nomura, R. Rodríguez-Guzmán, and L. M. Robledo, Phys. Rev. C **101**, 044318 (2020).
[29] J. Ferretti, J. Kotila, R. I. Magana Vsevolodovna, and E. Santopinto, Phys. Rev. C **102**, 054329 (2020).
[30] R. Álvarez-Rodríguez, P. Sarriguren, E. Moya de Guerra, L. Pacearescu, A. Faessler, and F. Šimkovic, Phys. Rev. C **70**, 064309 (2004).
[31] P. Sarriguren, Phys. Rev. C **91**, 044304 (2015).
[32] J. M. Boillos and P. Sarriguren, Phys. Rev. C **91**, 034311 (2015).
[33] P. Pirinen and J. Suhonen, Phys. Rev. C **91**, 054309 (2015).
[34] F. Šimkovic, V. Rodin, A. Faessler, and P. Vogel, Phys. Rev. C **87**, 045501 (2013).
[35] M. T. Mustonen and J. Engel, Phys. Rev. C **93**, 014304 (2016).
[36] J. T. Suhonen, Front. Phys. **5**, 55 (2017).
[37] A. Ravlić, E. Yüksel, Y. F. Niu, and N. Paar, Phys. Rev. C **104**, 054318 (2021).
[38] K. Yoshida, Y. Niu, and F. Minato, Phys. Rev. C **108**, 034305 (2023).
[39] K. Langanke and G. Martínez-Pinedo, Rev. Mod. Phys. **75**, 819 (2003).
[40] S. Yoshida, Y. Utsuno, N. Shimizu, and T. Otsuka, Phys. Rev. C **97**, 054321 (2018).
[41] T. Suzuki, S. Shibagaki, T. Yoshida, T. Kajino, and T. Otsuka, Astrophys. J. **859**, 133 (2018).
[42] F. T. Avignone, S. R. Elliott, and J. Engel, Rev. Mod. Phys. **80**, 481 (2008).
[43] J. Engel and J. Menéndez, Rep. Prog. Phys. **80**, 046301 (2017).
[44] M. Agostini, G. Benato, J. A. Detwiler, J. Menéndez, and F. Vissani, Rev. Mod. Phys. **95**, 025002 (2023).
[45] T. Otsuka, A. Arima, and F. Iachello, Nucl. Phys. A **309**, 1 (1978).
[46] T. Otsuka, A. Arima, F. Iachello, and I. Talmi, Phys. Lett. B **76**, 139 (1978).
[47] T. Mizusaki and T. Otsuka, Prog. Theor. Phys. Suppl. **125**, 97 (1996).
[48] K. Nomura, N. Shimizu, and T. Otsuka, Phys. Rev. Lett. **101**, 142501 (2008).
[49] K. Nomura, N. Shimizu, and T. Otsuka, Phys. Rev. C **81**, 044307 (2010).
[50] K. Nomura, T. Otsuka, N. Shimizu, and L. Guo, Phys. Rev. C **83**, 041302(R) (2011).
[51] K. Nomura, N. Shimizu, D. Vretenar, T. Nikšić, and T. Otsuka, Phys. Rev. Lett. **108**, 132501 (2012).
[52] K. Nomura, T. Nikšić, and D. Vretenar, Phys. Rev. C **93**, 054305 (2016).
[53] K. Nomura, R. Rodríguez-Guzmán, and L. M. Robledo, Phys. Rev. C **99**, 034308 (2019).
[54] K. Nomura, Phys. Rev. C **105**, 044306 (2022).
[55] K. Nomura, L. Lotina, R. Rodríguez-Guzmán, and L. M. Robledo, Phys. Rev. C **106**, 064304 (2022).
[56] K. Nomura, Phys. Rev. C **105**, 044301 (2022).
[57] T. Nikšić, N. Paar, D. Vretenar, and P. Ring, Comput. Phys. Commun. **185**, 1808 (2014).
[58] A. Bjelčić, T. Nikšić, and Z. Drmač, DIRHBspeedup, https://github.com/abjelcic/DIRHBspeedup.git.
[59] T. Nikšić, D. Vretenar, and P. Ring, Phys. Rev. C **78**, 034318 (2008).
[60] Y. Tian, Z. Y. Ma, and P. Ring, Phys. Lett. B **676**, 44 (2009).
[61] J. F. Berger, M. Girod, and D. Gogny, Nucl. Phys. A **428**, 23 (1984).
[62] S. Teeti and A. V. Afanasjev, Phys. Rev. C **103**, 034310 (2021).
[63] K. Nomura, D. Vretenar, and B.-N. Lu, Phys. Rev. C **88**, 021303(R) (2013).
[64] K. Nomura, D. Vretenar, T. Nikšić, and B.-N. Lu, Phys. Rev. C **89**, 024312 (2014).
[65] K. Nomura, T. Nikšić, and D. Vretenar, Phys. Rev. C **97**, 024317 (2018).
[66] A. Bohr and B. R. Mottelson, *Nuclear Structure* (Benjamin, New York, 1975).
[67] P. Ring and P. Schuck, *The Nuclear Many-Body Problem* (Springer, Berlin, 1980).
[68] F. Iachello and P. Van Isacker, *The Interacting Boson-Fermion Model* (Cambridge University Press, Cambridge, UK, 1991).
[69] O. Scholten, Prog. Part. Nucl. Phys. **14**, 189 (1985).
[70] I. Morrison, A. Faessler, and C. Lima, Nucl. Phys. A **372**, 13 (1981).
[71] J. N. Ginocchio and M. W. Kirson, Nucl. Phys. A **350**, 31 (1980).
[72] F. Dellagiacoma, Beta decay of odd mass nuclei in the interacting boson-fermion model, Ph.D. thesis, Yale University, 1988.
[73] Brookhaven National Nuclear Data Center, http://www.nndc.bnl.gov.
[74] P. D. Duval and B. R. Barrett, Phys. Lett. B **100**, 223 (1981).
[75] N. Stone, At. Data Nucl. Data Tables **90**, 75 (2005).
[76] A. Griffiths and P. Vogel, Phys. Rev. C **46**, 181 (1992).
[77] O. Civitarese and J. Suhonen, Phys. Rev. C **58**, 1535 (1998).
[78] O. Moreno, R. Álvarez-Rodríguez, P. Sarriguren, E. M. de Guerra, F. Šimkovic, and A. Faessler, J. Phys. G: Nucl. Part. Phys. **36**, 015106 (2009).
[79] S. Goriely, S. Hilaire, M. Girod, and S. Péru, Phys. Rev. Lett. **102**, 242501 (2009).